Generation of Rossby waves off the Cape Verde peninsula; role of the coastline

Jérôme Sirven[1], Juliette Mignot[1], and Michel Crépon[1]

[1]LOCEAN Laboratory, CNRS-IRD-Sorbonne Universités-MNHN,Paris, France

Correspondence: Jérôme Sirven (jerome.sirven@locean-ipsl.upmc.fr)

Abstract. In December 2002 and January 2003 satellite observations of Chlorophyll showed a strong coastal signal along the west african coast between $10°$ and $22°$ N. In addition, a wavelike pattern with a wavelength of about 750 km was observed from December 20th 2002 and was detectable for one month in the open sea, south west to the Cape Verde peninsula. Such a pattern suggests the existence of a locally generated Rossby wave which slowly propagated westward during this period. This hypothesis was confirmed by analyzing sea surface height provided by satellite altimeter during this period. To decipher the mechanisms at play, a numerical study based on a reduced gravity shallow water model has first been conducted. A wind burst, broadly extending over the region where the offshore oceanic signal is observed, is applied during 5 days. A Kelvin wave quickly develops along the northern edge of the cape, then propagates and leaves the area in a few days. Simultaneoulsly, a Rossby wave whose characterisics seem similar to the observed pattern forms and slowly propagates westward. The existence of the peninsula limits the extent of the wave to the north. The spatial extent of the wind burst determines the extent of the response and correspondingly the time scale of the phenomenon (about 100 days in the preent case). When the wind burst has a large zonal and small meridional extent, the behaviour of a wave to the north of the peninsula differs from that to the south. These results are corroborated and completed by an analytical study of a linear reduced gravity model using a non-Cartesian coordinate system. This system is introduced to evaluate the potential impact of the coastline shape. The analytical computations confirm that a period around 100 days can be associated with the observed wave considering the value of the wavelength; they also show that the role of the coastline remains moderate at such time scales. On the contrary, when the period becomes shorter (smaller than 20-30 days), the behaviour of the waves is modified because of the shape of the coast. South of the peninsula, a narrow band of sea isolated from the rest of the ocean by two critical lines appears. Its meridional extent is about 100 km and Rossby waves could propagate there towards the coast.

1 Introduction

Eastern Boundary Upwelling Systems (EBUS) — let us quote the California, Humboldt, Canary and Benguela upwelling systems — constitute an ubiquitous feature of the coastal ocean dynamics, which has been extensively studied. They are biologically very productive thanks to a transport of nutrients from deep ocean layers to the surface, which favors the bloom of phytoplanktons. Consequently they present a strong signature, which is detectable by ocean color satellite sensors (see for example Lachkar and Gruber 2012, 2013).

The dynamics of EBUS has first been studied with conceptual models. Upwellings are created by alongshore equatorward winds (Allen, 1976, McCreary et al., 1986) generating an offshore Ekman transport, which is compensated by a vertical transport at the coast in order to satisfy the mass conservation. The near shore pattern of the upwellings is affected by the baroclinic instability mechanism which is associated with the coastal current system and produces eddies and filaments (Marchesiello

5 et al., 2003). Lastly wind fluctuations modulate the upwelling intensity by generating Kelvin waves propagating poleward (Moore, 1968; Allen, 1976; Gill and Clarke, 1974; Clarke, 1977, 1983; McCreary, 1981).

At a given frequency, there is a critical latitude poleward of which Kelvin waves no longer exist and are replaced by Rossby waves propagating westward (Schopf et al., 1981; Clarke, 1983; McCreary and Kundu, 1985). The critical latitude decreases when the wave period shortens (Grimshaw and Allen, 1988) or when the coastline angle with the poleward direction increases

10 (Clarke and Shi, 1991). This latter property suggests that the shape of the coast has an impact on the upwellings.

Using a high-resolution 3D numerical model, Batteen (1997) then Marchesiello et al. (2003) confirmed that the shape of the coastline actually plays a role on the upwelling pattern. However they did not investigate by which mechanisms they are driven. In particular they did not try to confront their results with the theoretical investigations of Crépon et al. (1982, 1984) who analyzed the mechanisms responsible for this behaviour. Using an f-plane model, these authors showed that a cape modifies

15 the characteristics of the upwelling, its intensity being less on the upwind side of the cape than on the downwind side. However they did not investigate what occurs in the open sea up to 1000 km from the coast and which role could play the β effect.

The role of the forcing has also been investigated, both from observational and theoretical viewpoints. Enriquez and Friehe (1995) computed the wind stress and wind stress curl off the California shelf from aircraft measurements and showed, thanks to numerical experiments with a two layer model and an analytical study, that a non zero wind stress curl expands the horizontal

20 extent of upwelling offshore; it increases from 20-30 km to 80-100 km. The importance of the wind stress curl, which generates a strong Ekman pumping, were first emphasized by Richez et al., (1984) and later by Pickett and Paduan (2003) then Castelao and Barth (2006). They could establish that the Ekman pumping and the Ekman transport due to the alongshore winds have a comparable importance in the California Current area or off Cabo Frio in Brazil. These works did not study what occurs beyond 100 km from the coast.

25 In the present paper, we study the role of wind stress and coastline geometry in generating mesoscale anomalies offshore, up to a distance of 500-1000 km off the coast. Both a numerical and an analytical point of view are adopted. The departure point is the observation of a wave-like pattern on Chlorophyll satellite observations off the Senagalese coast, in the region of the Sénégalo-Mauritanian upwelling (see Lathuillière et al., 2008, and Farikou et al., 2015 to find further information about the Chl-a variability and the upwellings off the west African coast, Capet et al., 2017 for a recent analysis of the small scale

30 variability close to the Senegal and Gambia coasts, and Kounta et al., 2018 for a detailed study of the slope currents along west Africa). Attention is focused on offshore mesoscale activity associated with the upwelling, a recurrent feature of upwelling systems (see Capet et al., 2008 a, b). The alongshore activity, which has received much more attention (see for example Diakhaté et al., 2016 and the references herein) is not studied.

The paper is articulated as follows. Observations of Chlorophyll in 2002-2003 off the west African coast are shown and described in section 2. In section 3, a numerical study with a nonlinear reduced gravity shallow water model on the sphere with a single active layer is conducted; it shows that a wind stress anomaly active during a few days can generate a pattern that seems very similar to the observed one. The impacts of the wind anomaly extent and coastline geometry are also briefly studied. In section 4, a theoretical analysis of the wave dynamics in the vicinity of a cape is conducted to confirm and enlarge upon the results obtained in the previous section, using a linear shalow water model in a non-Cartesian coordinate system.

2 Observation of a wave off the Cape Verde peninsula from an ocean color satellite sensor.

The Senegalo-Mauritanian upwelling off the west coast of Africa forms the southern part of the Canary upwelling system. This region has been intensively studied by analysis of SeaWiFS ocean-color data and AVHRR sea-surface temperature as reported in Demarcq and Faure (2000), and more recently by Sawadogo et al. (2009), Farikou et al. (2013, 2015), Ndoye et al. (2014), and Capet et al. (2017). These studies indicate that the presence of an intense upwelling is attested by ocean-color and sea-surface temperature signals. Moreover this upwelling shows a strong seasonal modulation. It starts to intensify in October, reaches its maximum in April and slows down in June. Very high chlorophyll-a concentration are observed near the coast where the maximum is reached. However the concentration rapidly decreases offshore (Farikou et al., 2013, 2015; Sawadogo et al., 2009), suggesting that the upwelling extent and the eddy activity in this region is less than in other upwelling systems like the Californian Upwelling system (Marchesiello and Estrade, 2009, Capet et al., 2017).

From December 20th 2002 up to January 8th 2003, a strong chlorophyll signal was observed along the African coast on SeaWIFs satellite images, between 10°N and 22°N, indicating an intense biological activity. In addition, a well-defined "sine-like" pattern (circled in Figure 1) was observed on ten images taken at ten non-consecutive different days, which excludes a possible artifact due to image processing. This pattern is located between 12°N and 14°N east of 20°W and extends offshore up to 22°W in a region which is off the coastal upwelling zone. West of 20°W the signal seems to have a larger meridional extent, reaching 16°-17°N (see panel 3).

This pattern, which broadly keeps the same form during a twenty day interval, slowly progresses westward at a speed not exceeding 5 cm s^{-1} (a more precise estimation of the speed from the observations is quite hazardeous). After January 8th 2003, a cloudy period of several days occurred, which prevented satellite observations. At the end of this episode (January 15th) the "sine" pattern was no longer visible. This episode might be the signature of a Rossby wave propagating westward. As this phenomenon lasts at least one month, its typical time-scale is expected to range between one and a few months.

To corroborate this hypothesis, we analyzed the Sea Surface Height (hereafter SSH) obtained from AVISO satellite altimeter data for the corresponding period (December 2002 - January 2003). Hoevmuller diagrams are shown at 12°, 13.5°, 15°, and 16.5° in figure 2; they clearly confirm the existence of a Rossby wave propagating westwards with a velocity of about 4.5 cm s^{-1}. The amplitude of this wave becomes smaller northwards: it peaked at 13 cm between 12° and 13.5° but did not exceed 7 cm at 16.5°. The wavelength is around 700 km, comparable with the extent of the Chlorophyll signal.

An enhanced chlorophyll concentration, as seen by the satellite sensor, is the signature of growing phytoplankton. A local development of phytoplankton benefits from an increase of the nutrient concentration in the surface layers of the ocean. The latter may be generated by an enhanced mixing in the surface layers associated with an increased turbulence due to the Kelvin or Rossby wave activity and by the vertical velocity associated with the divergent Rossby waves. Another possible process explaining this growth could be the advection linked with Rossby waves – they create a current anomaly which can transport nutrients and phytoplankton from the upwelling area where they are highly concentrated. However, this mechanism is slow; for a current anomaly of 5 cm s^{-1}, the transport of a parcel of fluid over 500 km – less than the zonal extent of the offshore pattern – would need about one year.

The signal along the coast is also modulated by coastal Kelvin waves propagating northwards. Clarke and Shi (1991) showed that they can propagate when their angular frequency is larger than a critical angular frequency $\omega_c = c\beta\cos\Theta/2f_0$. In this formula Θ is an angle taking into account the tilt of the coastline with a meridian, c a typical velocity of a baroclinic mode and f_0 and β the usual parameters linked to the Earth's rotation. These authors found that ω_c ranges between 84.69 and 115.2 days around the Cape Verde peninsula (see their table 2a). These values are close to the characteristic time scales we expect here.

The existence of a long period divergent baroclinic Rossby wave, evidenced by the AVISO satellite altimeter data of the SSH, can explain the offshore sine-like pattern described here. To investigate the mechanism of emergence of this wave and analyze its properties, we first describe numerical experiments made with a numerical shallow water model. They help us see how such a wave is created and elucidate its nature. Then, a theoretical analysis is presented in order to understand how the Kelvin and Rossby waves behave when the coast presents a cape and to complete the interpretation of the numerical experiments. A wide range of periods is explored, going from 10 days to one year.

3   Numerical study

3.1   The model

The numerical model is a reduced gravity model on the sphere with one active layer of thickness h. It extends over an infinite layer at rest. The velocity $\mathbf{v}$ in the active layer and the thickness h verify the equations

$$\partial_t h + \mathrm{div}(h\mathbf{v}) = 0 \tag{1}$$

and

$$\partial_t \mathbf{v} + (\mathrm{rot}\mathbf{v} + f)\mathbf{n} \times \mathbf{v} = -\mathbf{grad}\Phi + \frac{\boldsymbol{\tau}_0}{h} - \frac{r}{h}\mathbf{v} + \nu\Delta_H\mathbf{v} \tag{2}$$

where $\mathbf{n}$ is a vector normal to the Earth's surface and $\mathrm{rot}\mathbf{v} = (\nabla \times \mathbf{v}).\mathbf{n}$. The function Φ is equal to $g^\star h + \mathbf{v}^2/2$ where $g^\star$ is the reduced gravity.

We assume for simplicity that the vector $\boldsymbol{\tau}_0$, which represents the surface wind stress divided by the ocean density, derives from a potential $\phi_0(x,y)$: $\boldsymbol{\tau}_0 = -\mathbf{grad}\phi_0$ (implying an irrotational mean wind). This hypothesis allows us to compute explicitly the obtained mean state. Indeed $\mathbf{v} = \mathbf{0}$ and $g^\star h_0^2/2 = -\phi_0 + C_0$ is an obvious solution of the previous system (the

constant C_0 is determined by using the fact that the mean value of h_0 remains unchanged during the integration). It will also facilitate the analytical computations made in the next section. A more complex set-up could be used for the numerical experiments but it will be seen below that this one suffices.

3.2 Numerical resolution

5 The model domain is closed and centered at $15°$N, the latitude of the Cape Verde peninsula; it has a latitudinal extent of $20°$ and a longitudinal extent of $30°$. The peninsula is modeled as indicated in Fig. 4 in order to mimic the geometry of the coast of Senegal (simplified and smoothed). The mean value of h_0 is equal to 200 m and the reduced gravity $g^\star$ to 0.02 m s^{-2}. Consequently the Rossby radius of deformation $R_0 = \sqrt{g^\star h_0}/f_0$ at the latitude of the Cape Verde is equal to 53 km.

The previous equations are solved by finite differences on a C-mesh on the sphere, the mesh size being equal to $(1/12)°$ in 10 longitudinal and latitudinal directions. The spatial scheme preserves enstrophy, following Sadourny (1975). No slip boundary conditions are applied everywhere (including along the artificial boundaries which limit the open ocean). There is no added dissipation in the continuity equations and mass is conserved by the numerical scheme. The time integration is performed using a leapfrog scheme with a time step of 300 seconds. The viscosity ν and the coefficient r of equation (2) are respectively equal to 28 m^{2}s^{-1} and 8×10^{-5} m s^{-1} ($h/r \simeq 1$ month). More details can be found in Février et al. (2007) where the two layer 15 version of this model is described.

3.3 Numerical set-up of the model

In Figure 3 the mean wind for the considered period (December 2002-January 2003) is shown. It exemplifies the situation which is normally found in this region. The wind regularly blows from the north-north-east with a velocity ranging from 4 to 8 m s^{-1}. To take this into account, a constant mean wind stress of amplitude equal to 0.06 N m^{-2} (corresponding to a mean 20 wind velocity of about 5 m s^{-1} and a value of τ_0 equal to 6×10^{-5} m^2 s^{-2}) and oriented along a south-south-west direction is applied from rest during four years, until a stationary mean state, which verifies the theoretical relation given in section 3.1, is reached.

As shown by Figure 3, a wind anomaly was active when the wave of Figure 1 begins to be observed. This anomaly obviously is transient, but to the south of the Cape Verde, it mainly points southwards. To represent this situation in a simplified way, 25 we defined in a first experiment a north-south wind stress anomaly which extends over approximately 500 km and whose maximum is still equal to 0.06 N m^{-2}. This anomaly is applied during five days (see Fig. 4 first panel). The integration is continued during 45 days, after the anomaly has disappeared.

To explore the sensibility of the model response to the wind anomaly, others wind anomalies were applied (see below, in particular Figures 6 to 8). The results obtained for these anomalies are discussed in the next section.

3.4 Numerical results

After the wind stress anomaly corresponding to the first experiment has vanished, the subsequent states of the ocean are shown every five days in Fig. 4 in terms of the active layer thickness. A coastal Kelvin wave forms north of the cape and quickly propagates along the coast. After 5 days, it has already gone beyond 25° N and after 10 days only the remains of the wave are still visible. South of the cape, a well marked (Rossby) wave develops. Its size matches more or less the size of the wind stress anomaly. It slowly propagates westwards with a velocity of about 4 cm s^{-1}. The amplitude of the wave decreases quickly because of the large value of h/r. The minimum value of h is about -3.5 m when the wind ceases (second panel) and reaches only -2 m after 25 days (seventh panel).

These characteristics are actually those of a Rossby wave locally generated by a wind anomaly, then freely propagating in the open ocean. The wavelength of this wave is about 750 km ($k_R \simeq 0.84 \times 10^{-5}$ m^{-1}). Such a value is compatible with the theoretical study presented in section 4 when the period of the wave is about 100 days. This modeled response to a wind stress anomaly also matches the satellite observed signal described in the previous section. It thus suggests that the latter is the consequence of the existence of Rossby wave generated by a wind burst.

Though the duration of the wind burst is short in our numerical experiment (5 days), the response of the system privileges a much longer time scale, exceeding 2 months. This result is not inconsistent. Indeed the Fourier transform of a rectangular pulse is the sine-cardinal function. It thus contains a significant amount of energy at low frequencies and thus can generate a low frequency response like the one observed here.

Figure 5 shows the results obtained in a similar experiment in which the cape is absent. The response of the model is very similar: in the area of the wind anomaly, a Kelvin wave forms then quickly desappears whereas a more persistant Rossby wave slowly propagates westward. However the meridional extent of the Rossby wave is broader east of 18° W, in the area where previously was the cape. This suggests that the cape simply limits the extent of the wave northward but does not modify its dynamics. The theoretical study of section 4 will confirm that the role of the cape remains moderate at low frequency.

A question arises: why does the wave have such a wavelength ? Numerical experiments clearly show that the longitudinal wavelength is defined by the spatial scale of the forcing anomaly. This is first illustrated in Figure 6, which shows the response of the model to a wind burst whose extent is four times smaller than the initial wind burst of Figure 4. The latitudinal and longitudinal extent of the model response are approximately divided by two as expected. No Kelvin wave of significant amplitude is generated because there is no longer wind anomalies at the coast; indeed, the centre of the wind anomaly is unchanged in comparison with the reference experiment. We will show in section 4 that the period associated with the wave are increased when the wavelength is reduced (reaching approximately 150 days).

Two supplementary experiments (Figures 7 and 8) have been made, in which a wind burst of large longitudinal (about 1000 km) and small latitudinal (about 100 km) extent is applied during 5 days; the anomaly is centered at 14°N in one case and 17°N in the other (see the first panel in Figures 7 and 8). These anomalies create a Rossby wave with a large zonal extent. However the response of the model differs in the two cases. When the anomaly is located south of the cape, a Kelvin wave is

generated and a negative anomaly appears between $26°$ and $20°$W. However no positive anomaly with a comparable amplitude can be seen closer to the coast. A weak signal appears after day 20 but its extent is very small and its amplitude is four times smaller than the amplitude of the anomaly observed around $25°$-$27°$W. South of $14°$, a wave of small amplitude is created and propagates southward. Its latitudinal wavelength is comparable with the latitudinal extent of the wind anomaly. When the wind
5 anomaly is located north of the cape, a negative anomaly appears between $26°$ and $20°$W as previously; besides, a positive anomaly can be seen from day 5 and its amplitude is half the amplitude of the signal observed around $25°$-$27°$W.

Clearly the response of the model close to the cape depends on the location of the wind anomaly, north or south of the cape. When the latter acts south of the cape, the anomaly which forms around $15°$W is small and quickly desappears; a wave which propagates southward seems to prevent its existence. On the contrary, when the wind anomaly acts north of the cape, an
10 anomaly forms around $15°$W and gets stuck in this place; the wave which propagates southward still exists but its amplitude is about twice samller than in the previous case. In the next section, we analytically investigate this dissymmetric behaviour in an idealized case.

4   Analytical study

In this section, we aim at understanding if the coastline may influence the propagation of the Rossby waves which are created
15 close to the coast and propagate towards the open sea. The impact of the coastline has been investigated by Crépon and Richez (1984), Clarke (1977), and Clarke and Shi (1991) for the Kelvin waves using an analytical approach. Here we focus on the Rossby waves; as we consider an area which extends up to about 1000 km from the coast, we have to generalize the approach followed by Clarke and Shi, which introduced a local system of coordinates dependent of the coastline to study Kelvin waves along an irregular coastline. We try to answer the following questions:
20   a) Are there time scales for which the impact of the coastline (small in the numerical experiments) becomes more important ?

b) A dissymmetry between the response north and south of the Cape was visible in the numerical experiments; can this dissymmetry be dependent on the existence of the Cape ?

The analysis begins by defining and building a system of coordinates that permits to follow the coastline geometry. This
25 procedure is a standard one in mathematics when boundaries are complex; indeed the the boundary conditions can be simply written, which constitutes a substantial advantage. however, it has a drawback: the differential equations which characerize the problem become slightly more complex because they must include geometrical factors that take into account the deformations associated with the new system of coordinates. This drawback is small in comparison with the advantage.

When these new equations are established, staightforward calculations are made to obtain a unique partial differential equa-
30 tion (equation (7)), which characterizes the evolution of η (the thickness of the active layer). This equation is a wave equation. Consequently the ray theory (or equivalently the WKB method) can be applied. When the forcing terms are neglected, this yields a first order nonlinear differential equation (equation (11). No new ideas are introduced after this. We just rewrite equa-

tion (11) by introducing new notations, in order to facilitate its study and the presentation of the results (end of paragraph 4.2). We then describe the results when the tranport along the coast is much larger than the transverse transport (section 4.3).

4.1 A model for the Kelvin and Rossby waves

We consider a reduced gravity shallow water model in the β plane forced by a constant wind stress which derives from a
5 potential $\phi_0(x,y)$ ($\boldsymbol{\tau}_0 = -\mathbf{grad}\phi_0$), as in section 3. Numerical integrations have shown that the exact solution $\mathbf{v} = \mathbf{0}$ and $g^\star h_0^2/2 = -\phi_0 + C_0$ is actually obtained after a few year integration (see section 3.1 and 3.3).

If an anomaly (τ_x, τ_y) is added to the mean forcing $\boldsymbol{\tau}_0$, a perturbation is generated; it is characterized by a *depth anomaly h* (the thickness of the first layer is now $h_0 + h$) and a velocity $\mathbf{v}$. A linear approximation is sufficient to study the first steps of the evolution of the perturbation if the forcing anomaly remains moderate. The anomaly (τ_x, τ_y) can be written in terms of a
10 potential $\phi(x,y,t)$ and a stream function $\psi(x,y,t)$,

$$
\begin{aligned}
\tau_x &= -\partial_x\phi - \partial_y\psi \\
\tau_y &= -\partial_y\phi + \partial_x\psi
\end{aligned}
\tag{3}
$$

so that the divergent part of the forcing is given by $-\Delta\phi$ and the rotationnal part by $\Delta\psi$.

The equations verified by *the anomalies h and $\mathbf{v}$* are thus:

$$
\begin{aligned}
h_0\partial_t u - f h_0 v + \partial_x(g^\star h_0 h + \phi) &= \nu h_0 \Delta_H u - ru - \partial_y\psi \\
h_0\partial_t v + f h_0 u + \partial_y(g^\star h_0 h + \phi) &= \nu h_0 \Delta_H v - rv + \partial_x\psi \\
\partial_t h + \partial_x(h_0 u) + \partial_y(h_0 v) &= 0
\end{aligned}
\tag{4}
$$

15 The role of the diffusion and dissipation will not be considered below – a smoothing and damping of the solution is expected when it is taken into account. The previous system may be further simplified by introducing the zonal and meridional transports $T_x = h_0 u$ and $T_y = h_0 v$ and a potential η equal to $g^\star h_0 h + \phi$. It becomes

$$
\begin{aligned}
\partial_t T_x - f T_y + \partial_x\eta &= -\partial_y\psi \\
\partial_t T_y + f T_x + \partial_y\eta &= \partial_x\psi \\
\partial_t\eta + c^2[\partial_x T_x + \partial_y T_y] &= \partial_t\phi
\end{aligned}
\tag{5}
$$

where $c = \sqrt{g^\star h_0}$ is a function of x and y.

20 These equations apply inside the ocean domain, whatever its shape. A boundary condition is added along the domain frontier (the normal transport vanishes) but the latter is difficult to handle when the shape of the coast is complex. Lastly, the spatial mean value of the depth anomaly h remains null.

The propagation of a Kelvin wave along the eastern boundary and the possible generation of Rossby waves can be studied by using system (5). Here, we consider an eastern boundary whose angle with the meridians smoothly varies and we seek to
25 understand how these variations may affect the wave dynamics. We consider only the case of a cape even though the method

could be applied in other cases. A coordinate change is made in order to "straighten the coast" and therefore have a simple boundary condition; equations (5) are correspondingly modified to match the new coordinates.

A new orthogonal system of coordinates $X = \mathcal{X}(x,y)$ and $Y = \mathcal{Y}(x,y)$ is thus introduced such that the eastern boundary is now defined by the simple equation $X = 0$ (rather than a complex one such as $f(x,y) = 0$). In the local orthonormal basis $\mathbf{e}_X, \mathbf{e}_Y$ associated with this coordinates system, the line element $\mathrm{d}\mathbf{l}$ reads

$$\mathrm{d}\mathbf{l} = a\,\mathrm{d}X\,\mathbf{e}_X + b\,\mathrm{d}Y\,\mathbf{e}_Y$$

where a and b are geometrical factors which convey the stretching of the coordinates along orthogonal directions (note that the relations

$$a = \sqrt{(\partial_X x)^2 + (\partial_X y)^2} \quad \text{and} \quad b = \sqrt{(\partial_Y x)^2 + (\partial_Y y)^2}$$

where the initial coordinates x and y are now functions of the new coordinates X and Y are used to compute a and b).

Such a coordinate change is illustrated in figure 9 for a cape protruding into the sea over a distance of 80 km. Only half of the symmetric domain is shown. The initial coordinates x and y are the zonal and meridional coordinates; the new coordinates X and Y are represented in the original system and some of their values are indicated. Other coordinate changes would be possible. The corresponding geometrical factors a and b are shown in figure 10. They differ from 1 respectively in a close neighbourhood and to the west of the cape (a is equal to 0.1 around the extremity of the cape whereas b reaches 40 at 300 km west of the cape). A detailed study of this example will be presented in subsection 4.3.

Using the coordinates (X, Y), system (5) becomes

$$
\begin{aligned}
\partial_t T_X - FT_Y + a^{-1}\partial_X \eta &= -b^{-1}\partial_Y \psi \\
\partial_t T_Y + FT_X + b^{-1}\partial_Y \eta &= a^{-1}\partial_X \psi \\
\partial_t \eta + (C^2/(ab))[\partial_X(bT_X) + \partial_Y(aT_Y)] &= \partial_t \phi
\end{aligned}
\tag{6}
$$

where F, C, T_X, T_Y are functions of X and Y corresponding to f, c, T_x and T_y (the notations for η, ϕ and ψ have not been changed to enhance the readability, but these functions also depend on X and Y).

Note that we use a more complex system than the traditional one which is used for the study of the Kelvin waves and which neglect the variations of the transport perpendicular to the coast :

$$
\left\{
\begin{aligned}
-FT_Y + a^{-1}\partial_X \eta &= -b^{-1}\partial_Y \psi \\
\partial_t T_Y + FT_X + b^{-1}\partial_Y \eta &= a^{-1}\partial_X \psi \\
\partial_t \eta + (C^2/(ab))[\partial_X(bT_X) + \partial_Y(aT_Y)] &= \partial_t \phi
\end{aligned}
\right.
$$

We use the complete system 6 because we study Rossby waves far from the coast, for which these hypotheses does not hold. Indeed, the previous simplified system leads to drop in equation (11) below two terms: $(1/b^2)(\partial_Y \theta)^2$ and $iF^2\partial_Y(a/(bF^2))\partial_Y \theta$. These terms include the geometrical factors a and b due to the coordinates change; and we precisely try to investigate which is the impact of such terms.

We now concentrate on processes whose time scale is much larger than one day. Moreover we consider only the evolution of free waves. This situation corresponds to the case numerically investigated in section 3 and illustrated in Figures (4 - 8): the wind stress anomaly that had created the depth anomalies has ceased to exert. With these hypotheses, system (6) can be reduced into the following equation which characterizes the evolution of η:

5 $$\partial_t \left[\eta - R_0^2 (\frac{1}{a^2} \partial_{XX}^2 \eta + \frac{1}{b^2} \partial_{YY}^2 \eta) \right] - \cdots$$

$$\cdots \frac{R_0^2}{ab} \left[F^2 \partial_X (\frac{b}{aF^2}) \partial_{tX}^2 \eta + \partial_Y F \partial_X \eta + F^2 \partial_Y (\frac{a}{bF^2}) \partial_{tY}^2 \eta - \partial_X F \partial_Y \eta \right] = 0 \tag{7}$$

where $R_0 = C/F$ is the Rossby radius. The boundary condition at the eastern coast now reads:

at $\quad X = 0, \quad b \partial_{tX}^2 \eta + a F \partial_Y \eta = 0$ (8)

for all $t > 0$ and Y. The details of the computations can be found in Appendix 1.

10 When a and b are close to 1 and the coast has a south-north orientation (see Figure 10) the new coordinates system is nearly similar to the original one; indeed F mainly depends on $Y \simeq y$ only and in those regions equation (7) thus simplifies:

$$\partial_t \left[\eta - R_0^2 (\partial_{XX}^2 \eta + \partial_{YY}^2 \eta) \right] - R_0^2 \left[\partial_Y F \partial_X \eta + F^2 \partial_Y (\frac{1}{F^2}) \partial_{tY}^2 \eta \right] = 0 \tag{9}$$

We recognize the equation characterizing the propagation of waves in the β plane ($\beta = \partial_Y F$) for a shallow water model. For a tilted coast the dependance of the Coriolis parameter as a function of X should be still taken into account. For spatial scales 15 much larger than R_0 and at low frequency, equation (9) can be further simplified. It becomes $\partial_t \eta - R_0^2 \partial_Y F \partial_X \eta = 0$ which simply models the westward propagation of long Rossby waves.

The coefficient b decreases as one gets closer to the cape (see Figure 10). An impact of the cape in the open sea may therefore be expected because of the terms proportional to $\partial_X (\frac{b}{aF^2}) \partial_{tX}^2 \eta$ and $\partial_X F \partial_Y \eta$ in equation (7).

4.2 Ray theory

20 When a wave propagates in a medium whose properties spatially change, it does not follow straight lines but more complex paths. Ray theory – or WKBJ approximation – is used to determine the paths followed by the waves in such a medium. It applies when the wavelength is smaller than the typical scale at which the properties of the medium vary. The spatial variations of the components k and l of the wavevectors are taken into account by introducing a complex function $\theta(X, Y) = \theta_R + i \theta_I$ such as $k = \partial_X \theta$ and $l = \partial_Y \theta$. The potential η is then equal to

25 $\eta = \eta_0(X, Y) \exp[i(\omega t + \theta(X, Y))]$ (10)

where it is assumed that $|\eta_0^{-1} \partial_X \eta_0| \ll |\partial_X \theta|$, $|k^{-1} \partial_X k| \ll |\partial_X \theta|$, $|\eta_0^{-1} \partial_Y \eta_0| \ll |\partial_Y \theta|$, $|l^{-1} \partial_l l| \ll |\partial_Y \theta|$. As required by the theory, these inequalities ensure that the wavelength is smaller than the typical scale of variation of the system, here conveyed by R_0, F and the coefficients a and b. Excepted in a very close vicinity of the cape (distance smaller than around ten kilometers)

and for the meridional wavelength in the area located between -50 and 50 km north and south of the cape and beyond 200 km west of the cape, these inequalities mean that several wave patterns must be visible in the considered domain. This condition is verified for the waves observed in the numerical experiments and for the waves considered below.

Considering these hypotheses, η is given from equation (10) in the neighbourhood of a point M_0 of coordinates (X_0, Y_0) by the approximate expression

$$\eta(X,Y) = \eta_0(X_0,Y_0)\exp[i(\omega t + k(X - X_0) + l(Y - Y_0))]$$

where $k = \partial_X\theta|_{M_0}$ and $l = \partial_Y\theta|_{M_0}$. The physical meaning of this solution is explicited by taking its real part:

$$\Re(\eta) = \eta_0(X_0,Y_0)e^{-k_I(X-X_0)-l_I(Y-Y_0)}\cos[\omega t + k_R(X - X_0) + l_R(Y - Y_0)]$$

The solution must not increase westward since it cannot become infinite, which implies $k_I < 0$. Note however that $k_I > 0$ is possible if this occurs only in a (small) bounded domain. For $k_R > 0$, the wave propagates westwards.

The values of k and l are obtained by computing the function θ from equations (7) and (8). After simplifying them by using the hypotheses above, we find that θ verifies the approximate (eikonal or Hamilton-Jacobi) equation

$$\left(1 + R_0^2\left[\frac{1}{a^2}(\partial_X\theta)^2 + \frac{1}{b^2}(\partial_Y\theta)^2\right]\right) - \cdots$$

$$\cdots \frac{R_0^2}{ab}\left[i F^2\partial_X(\frac{b}{aF^2})\partial_X\theta + i F^2\partial_Y(\frac{a}{bF^2})\partial_Y\theta + \partial_Y(\frac{F}{\omega})\partial_X\theta - \partial_X(\frac{F}{\omega})\partial_Y\theta\right] = 0 \tag{11}$$

with the boundary condition

$$ib\partial_X\theta + a(F/\omega)\partial_Y\theta = 0 \tag{12}$$

at $X = 0$.

To make the computations clearer we set
— $z_1 = (\partial_X\theta)R_0/a = kR_0/a$
— $z_2 = (\partial_Y\theta)R_0/b = lR_0/b$,
— $w_1 = (R_0/2b)\left[\partial_Y(\frac{F}{\omega}) + i F^2\partial_X(\frac{b}{aF^2})\right]$
— $w_2 = (R_0/2a)\left[-\partial_X(\frac{F}{\omega}) + i F^2\partial_Y(\frac{a}{bF^2})\right]$
and the problem (11) associated with the boundary condition (12) is rewritten as the following system :

$$\partial_Y(\frac{az_1}{R_0}) = \partial_X(\frac{bz_2}{R_0}) \tag{13}$$

$$1 + z_1^2 + z_2^2 - 2z_1w_1 - 2z_2w_2 = 0 \tag{14}$$

$$z_2 = -i\frac{\omega}{F}z_1 \quad \text{at} \quad X = 0 \tag{15}$$

At the boundary, equations (14) and (15) permit to determine the values of z_1 and z_2, hence of k and l. Indeed, the introduction of (15) in (14) leads to the equation

$$1 + (1 - \frac{\omega^2}{F^2})z_1^2 - 2z_1(w_1 - i\frac{\omega}{F}w_2) = 0$$

Setting $\xi = \sqrt{1 - (\omega/F)^2}$, this equation can be rewritten

5   $$J(\xi z_1) = \frac{1}{\xi}(w_1 - i\frac{\omega}{F}w_2) = W_R + iW_I \tag{16}$$

where $J(z) = \frac{1}{2}(z + \frac{1}{z})$ is the Joukowsky transform of z; W_R and W_I are given by the relations

$$
\begin{aligned}
W_R &= \frac{R_0 F}{2\xi} \times \frac{F}{\omega}\left[-\xi^2 \frac{1}{b}\partial_Y \frac{1}{F} + (1 - \xi^2)\frac{1}{a}\partial_Y(\frac{a}{bF})\right] \\
W_I &= \frac{R_0 F}{2\xi} \times \frac{1}{b}\partial_X(\frac{b}{aF})
\end{aligned}
$$

Equation (16) is the dispersion relation of the wave at the boundary. The Joukowsky transform of ξz_1 (or equivalently of $i\frac{F}{\omega}\xi z_2$) depends on the frequency ω, the mean state (through R_0), the latitude (through F) and the geometry of the coast
10   (through a and b).

The sketch in Figure 11, which shows the half complex plane $\Im(z) < 0$ (upper panel) and the complex plane $W = J(z)$ (lower panel), explicits how the Joukowsky transformation works. The inferior half plane has been chosen since we expect $k_I < 0$, or in other words $\Im(z) < 0$.

— When $W_I = \Im(W)$ is *positive*, the complex number ξz_1 such as $J(\xi z_1) = W = W_R + iW_I$ has a norm smaller than 1
15   (it corresponds to the gray areas in Figure 11). The wavelength is thus large ($\lambda > 2\pi\xi R_0/a$). If $W_R = \Re(W)$ is positive, the phase speed is negative (westward propagation).

— When $W_I = \Im(W)$ is *negative*, the complex number ξz_1 such as $J(\xi z_1) = W = W_R + iW_i$ has a norm larger than 1 (it corresponds to the white areas). The wavelength is thus small. If $W_R = \Re(W)$ is positive, the phase speed is still negative.

— When W_I *vanishes*, a situation which occurs when the coast is a straightline, the unique complex solution previously
20   found can cease to exist. Indeed, if $|W_R|$ is smaller than 1, there is *one complex* solution whose norm is equal to 1 (on the half circle in bold in Figure 11); and if $|W_R|$ is larger than 1, *two real* solutions are obtained (between $]-1,1[$ and outside this interval). The case ($W_I = 0$) is detailed in the next subsection.

At the coast, relation (15) determines z_2 when z_1 is known. It implies that

$$l_I = \frac{\omega}{F}\frac{b}{a}k_R \quad \text{and} \quad l_R = -\frac{\omega}{F}\frac{b}{a}k_I$$

25   For low frequencies ω/F is much smaller than 1 and l_I and l_R can be ignored. An approximate expression of the waves is

$$\eta(X,Y,t) = \eta_0(X_0,Y_0)e^{-k_I(X-X_0)}\cos(\omega t + k_R(X - X_0))$$

and the dynamics is controlled by the westward propagation of Rossby waves. For shorter periods, the situation may be more complex because the ratio $\omega b/(aF)$ may be close to 1. This effect is in agreement with the results obtained in section 3, where

a southward propagation of waves was observed in the open ocean, simultaneously with the westward progation of Rossby waves.

Knowing z_1 and z_2 along the coast, it is possible to continue the resolution of the problem (13-14) and compute explicitly the rays characterizing the propagation of the waves. An algorithm which fulfils this objective is described in appendix 2. However, under the supplementary assumption that $|T_X|$ remains much smaller than $|T_Y|$ up to a distance from the coast of about a few Rossby radius of deformation, approximate expressions for z_1 and z_2 can be obtained analytically. This also permits to initialize the algorithm described in appendix 2.

4.3 Analytical study for $|T_X| \ll |T_Y|$.

In this case, equation (15) which is exact at the coast $X = 0$ can also be used on a band of a few hundred kilometers off the coast and yields a good approximation of the solution (for a more detailed discussion, see Appendix 2). Consequently, equation (16) becomes valid over a domain which extends far off the coast in the open ocean. In this section, the consequences of this relation are briefly presented for a straight coastline, then investigated in detail for the cape shown in figure (9). In agreement with the hypotheses of the previous subsection, we assume that $\omega \ll F$ but the results and graphics will be produced up to the limit value $\omega = F$.

Case of a straight coastline. This case has been extensively studied in the literature — let us mention Richez et al. (1984), Grimshaw and Allen (1988), Clarke and Shi (1991), McCalpin (1995), Liu et al. (1998) — each article stressing a particular issue. Using the previously established equations, we summarize here known results about the existence of critical frequencies along an ocean boundary.

For a straight coastline following the south north direction, we have $X = x$ and $Y = y$; consequently $a = b = 1$ and F depends only on Y. Thus $W_I = 0$ and

$$2W_R = \frac{R_0\beta}{\omega}\frac{2\xi^2 - 1}{\xi}$$

where $\beta = \partial_Y F$.

In figure 12 (top panel), the coefficient W_R is shown at different latitudes as a function of the period. At 15° N, the critical value $W_R = 1$, which ensures the transition from a complex solution to two real solutions, is reached when the period is 140 days. The bottom panel shows the wavenumber as a function of the wave period computed from W_R for 10° N (black), 15° N (grey) and 20° N (light grey). When $W_R > 1$, a condition which is always fulfilled at low frequency (characteristic time longer than 125 days at 15°), equation (16) has two real solutions. If $W_R \gg 1$ these solutions are close to $2W_R \simeq R_0\beta/\omega$ and $1/2W_R \simeq \omega/(\beta R_0)$. Consequently, the wave number k is equal to either β/ω or $\omega/(\beta R_0^2)$ (see equation 16). This result proves the existence of Rossby waves, whose wavelength is either short or long. When the frequency increases, W_R decreases and eventually reaches the critical value 1. When W_R becomes smaller than 1, there are two complex conjugate solutions. The only acceptable solution has a *negative imaginary part* and conveys the existence of a Kelvin wave, trapped along the coastline and propagating northward. The absolute value of this imaginary part k_I is represented as a dashed curve in Figure 12 (bottom

panel). When the wave frequency is close to the critical value, k_I vanishes and consequently the Kelvin wave no longer exist. A Rossby wave with a significant amplitude can propagate westwards. At $15°$ N its wavelength will be around 300 km. The zonal velocity (phase speed) of this non dispersive wave is about 2.5 km/day. On the other hand, as l_R vanishes with k_I, the meridional velocity becomes infinite.

5 Similar results are obtained when the coast presents a constant angle θ with a meridian. The only change is that the critical frequency for which the wave regime changes is modified and depends on the tilt of the coast as indicated in Clarke and Shi (1991).

Case of a cape. The wave dynamics in a neighbourhood of the cape is characterized by the coefficients W_R and W_I which convey the effect of the coastline on the propagation of the wave. The coefficient W_R can be splitted into two terms; the first

10 one $\dfrac{R_0}{2b}\dfrac{2\xi^2-1}{\xi}\partial_Y\dfrac{F}{\omega}$ is similar to the term obtained from a straight coastline whereas the second one $\dfrac{R_0}{2a}\dfrac{1-\xi^2}{\xi}\partial_Y\dfrac{a}{b}$ explicits the role of the coast. It is large when ξ is small — in the frequency range where the model is valid, this means for wave periods going from ~ 10 days to a month — and when the deformation of the coastline is large. The existence of such a term was expected. When the angle of the coastline with a meridian increases, the impact of the latitudinal variations of the Coriolis parameter decreases along the path followed by the wave. It even vanishes when the coast becomes parallel to the equator.

15 These changes are taken into account by this term. On the contrary, at low frequency, the lengthening or shortening of the path followed by the wave becomes negligible because it occurs over a time which remains short in comparison with the period of the wave.

The variations of the coastline geometry also prevent the existence of two distinct solutions at low frequency. Indeed, W_I differs from 0 and consequently two complex solutions are obtained as explicited in Figure 11. If W_I is strictly negative (grey

20 area), the solution z is inside the half unit disk and k_R is small. If W_I is strictly positive, the solution is outside and k_R is large. The degeneracy of the equation thus desappears and a selection of the wavelength operates.

Figure 13 shows W_R for $T = 10, 20, 50,$ and 100 days and makes visible an interesting property. When the period T is equal to 10 days, a dissymmetry around the cape occurs: W_R is negative south and positive north of the cape. This dissymmetry weakens when the period increases. For $T = 20$ days, the area where W_R is negative is strongly reduced and for $T = 50$ days,

25 it has vanished. Since the signs of W_R and k_R are similar (see Figure 11 and the associated comments), a negative k_R is expected in this area and actually appears (see Figure 15)

Since W_I is nearly independent of the period in the considered frequency range, a single map suffices to describe it (Figure 14). W_I is positive everywhere except in an narrow area west of the cape (the isoline -0.2 is indicated and the bold line corresponds to $W_I = 0$). Figure 11 shows that the corresponding values of ξz_1 are smaller than 1. This suggests that this area

30 is occupied by waves whose wavelength is longer than everywhere else, a result which appears in Figure 15.

The maps of k_R and k_I (see Figures 15 and 16) show properties in agreement with the previous analysis. For periods shorter than 20 days, k_R becomes negative south of the cape. Consequently the waves no longer propagate westward towards the open sea, but eastward towards the coast. On the contrary, north of the cape the propagation occurs always westward, whatever the

frequency. At lower frequency this phenomenon is not observed. The coefficient k_I shows a smaller dependence as a function of the period. The shape of the Kelvin wave is modified close to the tip of the cape – its offshore extent is smaller since k_I is larger – but it still exists and propagates northwards.

Lastly, note that the order of magnitude predicted in Figure 12 for a straight coastline with a south north orientation are noticeably changed when the shape of the coast is taken into account. For a wavelength of about 700 km, the corresponding period was equal to approximately 150 days. Now, figure 15 shows that this wavelength are obtained in a large part of the domain for a period equal to 100 days. Note that this value is close to the values predicted by Clarke and Shi (1991) at the coast (between 84.69 and 115.2 days). Note also that, in a small area around the extremity of the cape (grey area), larger wavelengths are compatible with periods of about 100 days.

5 Conclusions

The analysis of SeaWiFS satellite observations of Chlorophyll showed a well marked signal along and off the west african coast, between $10°$ and $22°$ N, in winter (December to April). Along the coast the high concentration of Chlorophyll is associated with the offshore Ekman drift generated by the equatorward component of the trade wind, which forces an upward motion. Its variability is modulated by Kelvin wave propagating northwards. In December 2002 and January 2003 we observed a wavelike pattern in the open sea, which extends far away offshore, up to a distance of about 800 km off the coast. This signal was visible from 20 December 2002 and was detectable during approximately one month, south of the Cape Verde Peninsula.

This pattern suggested the existence of locally generated Rossby waves, which slowly propagated westward. Indeed such a wave can generate an elevation of the lower layers of the ocean corresponding to an upwelling of nutrient-rich water. The existence of this wave was confirmed by the study of the SSH signal coming from AVISO altimeter data. It evidenced a wave propagating westward with a velocity of about 4.5 cm s^{-1}. The existence of a Chlorophyll signal far from the coast – here extending up to 750 km west to the Cape Verde has to our knowledge never been described. This strongly differs from the coastal signals associated with Kelvin waves which have been previously carefully analyzed (see Diakhaté et al. 2016 and the references herein).

In this study we thus investigated the mechanisms which could lead to the existence of such a wave and analyzed the potential role of the cape, by first doing numerical experiments with a forced nonlinear model, then by analytically studying a linear reduced gravity model.

The numerical study, based on a reduced gravity shallow water model, showed that a Rossby wave similar to the observed pattern could be created by a wind burst broadly extending over the region where the oceanic signal was seen. This agreed with wind reanalysis of this period. In our experiments a longshore wind burst which lasted 5 days was used to generate the oceanic response. We showed that the spatial scale of the latter matches the spatial scale of the forcing. The time scale of the reponse, controlled by the wavelength (see below), is not that of the forcing (5 days) but much longer around 100 days for the first experiment.

The cape does not seem to modify the basic features of the wave dynamics. It mainly limits the extent of the wave to the north. However, when the wind burst has a large zonal extent (of about 1000 km) and a small meridional extent (not exceeding 100 km), the response of the model close to the cape depends on the location of the wind anomaly. When the latter acts south of the cape, the anomaly which forms around 15° W is small and quickly desappears; a wave which propagate southward seems to prevent its existence. On the contrary, when the wind anomaly acts north of the cape, an anomaly forms and remains around 15° W, without moving; a secondary wave which propagates southward still exist but desappears quickly.

The analytical study is new and extends the study of Clarke and Shi (1991) to the open sea up to a distance of about 1000 km away from the coast. It helps us interpret the numerical results and gives futher information. It first shows that a time scale around 100 days can be associated with the observed wave, considering the value of the wavelength (around 700 km). This value matches the critical value predicted by Clarke and Shi along the coast of Senegal, even though their model applied only at the coast when the angle defining the tilt of the coastline is not too large. It also shows that the role of the cape does not dramatically modify the dynamics of the system at such time scales.

On the contrary, when the period becomes shorter (smaller than 20-30 days), the waves behaves differently north and south of the cape, as suggested by the numerical experiments. For the studied set-up, Rossby waves can propagate eastwards, in a narrow band of the ocean whose latitudinal extent is about 100 km. We verified that this property vanished when the cape flattened (the period of the wave progressively becoming shorter). This strongly suggests that the wave dynamics in the vicinity of a cape – and the associated upwelling – depends on the geometry of the coastline for time scales shorter than one month. These changes no longer matter for longer time scales. Note that the behaviour difference predicted by the theory are not so important in the numerical experiments. This is not surprising since the geometry of the system is different in the numerical experiments.

This study thus suggests that offshore upwellings can be created or enhanced by Rossby waves. An example of such a phenomenom has been observed in the region off Senegal. This example is probably not unique. For instance Kounta et al. (2018) show patterns which provide clear evidence of an important Rossby wave activity to the south of the Cape Verde (see for example their Figure 10, which shows a climatology of the volume meridional transport). Observations will have to be pursued in this region and in other EBUS region to determine the importance of such events. However the observations of such structure by satellite requires several condition which are seldom occuring together. First we need a long period of observations without clouds, second a typical wind event able to generate the Rossby wave and third the existence of nutrients in the subsurface layers, which could enrich the surface layers.

An important problem is the detectability of these waves. Dealing with a reduced gravity model whose characteristics are fitting the observations, we found that the elevation of the interface probably does not exceed a few meters. The interface elevation facilitates the nutrient enrichment of the surface layers and consequently favours phytoplankton blooms. As the elevation of the interface is relatively small, the phytoplankton bloom is likely to occur only under very specific conditions such as a relatively small average thermocline depth or the presence of phytoplankton species capable of rapid growth, with a strong chlorophyll signature like diatoms. In fact, phytoplankton pigment retrieval from ocean color satellite observation

shows that the chlorophyll signal we observed is dominated by fucoxanthin, which is a signature of diatoms (Khalil et al, 2019, submitted)

Appendix A: Appendix A

Since we consider processes whose time scale is larger than a day, equations (6) can be simplified. We define a characteristic frequency ω_0 and a daily frequency F_d and assume that they verify $\epsilon = \omega_0/F_d \ll 1$. Setting $\omega_0 t = \tau$ and $F = F_d F_0$, the first two equations of system (6) become

$$
\begin{aligned}
\epsilon \partial_\tau T_X - F_0 T_Y &= R_X/F_d \\
\epsilon \partial_\tau T_Y + F_0 T_X &= R_Y/F_d
\end{aligned}
\tag{A1}
$$

with $R_X = -a^{-1}\partial_X \eta - b^{-1}\partial_Y \psi$ and $R_Y = -b^{-1}\partial_Y \eta + a^{-1}\partial_X \psi$. An elementary computation leads to the following relations

$$
\begin{aligned}
(\epsilon^2 \partial_{\tau\tau} + F_0^2)T_X &= (\epsilon \partial_\tau R_X + F_0 R_Y)/F_d \\
(\epsilon^2 \partial_{\tau\tau} + F_0^2)T_Y &= (\epsilon \partial_\tau R_Y - F_0 R_X)/F_d
\end{aligned}
\tag{A2}
$$

Considering our hypothesis, the terms of order 1 and ϵ can be kept in the previous equations and the terms of order ϵ^2 can be neglected. Consequently we can use the approximate relations

$$
\begin{aligned}
T_X &= F^{-2}(\partial_t R_X + F R_Y) \\
T_Y &= F^{-2}(\partial_t R_Y - F R_X)
\end{aligned}
\tag{A3}
$$

(We used the fact that $\epsilon F_d^{-1}\partial_\tau = F^{-1}\partial_t$ and $F_0 F_d = F$). Note that the terms $\partial_t R_X$ and $\partial_t R_Y$ are of order ϵ in comparison with the terms $F R_Y$ and $F R_X$.

We now introduce these equations in the last equation of system (6). This leads to a new equation

$$
\partial_t \eta + \frac{C^2}{ab}[\partial_X (\frac{b}{F^2}(\partial_t R_X + F R_Y)) + \partial_Y(\frac{a}{F^2}(\partial_t R_Y - F R_X))] = \partial_t \phi
\tag{A4}
$$

or equivalently

$$
\begin{aligned}
\partial_t \left[\eta - R_0^2(\frac{1}{a^2}\partial^2_{XX}\eta + \frac{1}{b^2}\partial^2_{YY}\eta)\right] - \\
\frac{R_0^2}{ab}\left[F^2 \partial_X(\frac{b}{aF^2})\partial^2_{tX}\eta + \partial_Y F \partial_X \eta + F^2 \partial_Y(\frac{a}{bF^2})\partial^2_{tY}\eta - \partial_X F \partial_Y \eta\right] = \partial_t \phi + R_\psi
\end{aligned}
\tag{A5}
$$

where $R_0^2 = C^2/F^2$ is the Rossby radius and R_ψ contains the forcing terms depending on ψ:

$$
R_\psi = -\frac{C^2}{ab}\left[\partial_X(\frac{1}{F^2})\partial_{tY}\psi + \partial_Y(\frac{1}{F^2})\partial_{tX}\psi + \partial_X(\frac{b}{aF}\partial_X \psi) - \partial_Y(\frac{a}{bF}\partial_Y \psi)\right]
$$

The vanishing of the velocity orthogonal to the coordinates is easily obtained from system (A3). With the same approximations, the condition $T_X = 0$ at $X = 0$ implies $\partial_t R_X + F R_Y = 0$ or equivalently

$$b\partial^2_{tX}\eta + aF\partial_Y\eta = -a\partial^2_{tY}\psi + bF\partial_X\psi \tag{A6}$$

for all $t > 0$ and Y.

5 When the forcing terms can be neglected, the previous relations simplify. They become respectively

$$\partial_t\left[\eta - R_0^2(\frac{1}{a^2}\partial^2_{XX}\eta + \frac{1}{b^2}\partial^2_{YY}\eta)\right] - \cdots$$
$$\cdots\frac{R_0^2}{ab}\left[F^2\partial_X(\frac{b}{aF^2})\partial^2_{tX}\eta + \partial_Y F\partial_X\eta + F^2\partial_Y(\frac{a}{bF^2})\partial^2_{tY}\eta - \partial_X F\partial_Y\eta\right] = 0 \tag{A7}$$

and at $X = 0$, for all $t > 0$ and Y

$$b\partial^2_{tX}\eta + aF\partial_Y\eta = 0 \tag{A8}$$

10 **Appendix B: Appendix 2**

A method to solve system (13-14) with the boundary condition (15) is presented here. It has been shown that the values of z_1 and z_2 are known on the boundary thanks to equation (16). We set

$$z_1 = z_1^0 + \tilde{z}_1 \quad \text{and} \quad z_2 = z_2^0 + \tilde{z}_2$$

where z_1^0 and z_2^0 verifies equation (14) and the condition $z_2^0 = -i(\omega/F)z_1^0$ everywhere. Consequently, z_1^0 verifies equation (16)

15 everywhere

$$J(\xi z_1^0) = W_R + iW_I$$

and can be computed on the ocean domain. The results of this computation are presented in section 4.3 (z_2^0 is also known thanks to the relation $z_2^0 = -i(\omega/F)z_1^0$).

Since z_1 and z_2 are known on the coast and z_1^0 and z_2^0 everywhere, $\tilde{z}_1$ and $\tilde{z}_2$ are known on the coast $X = 0$. It is now easy

20 to write the equations verified by $\tilde{z}_1$ and $\tilde{z}_2$.

$$\partial_Y(\frac{a\tilde{z}_1}{R_0}) - \partial_X(\frac{b\tilde{z}_2}{R_0}) = \partial_Y(\frac{az_1^0}{R_0}) - \partial_X(\frac{bz_2^0}{R_0}) = \mathcal{Z}_0 \tag{B1}$$

$$\tilde{z}_1^2 + 2\tilde{z}_1(z_1^0 - w_1) + \tilde{z}_2^2 + 2\tilde{z}_2(z_2^0 - w_2) = 0 \tag{B2}$$

with $\tilde{z}_1 = 0$ and $\tilde{z}_2 = 0$ for $X = 0$.

The variables $\tilde{z}_1$ and $\tilde{z}_2$ can be computed on a grid $(-i\Delta X, j\Delta Y)$ for $i = 0, 1, \ldots, N$, $j = -P, \ldots, -1, 0, 1, \ldots, P$. They are known for $X = 0$ ($i = 0$). We suppose that they have been computed for $i > 0$ (values $\tilde{z}_{1,i,j}$ and $\tilde{z}_{2,i,j}$) and show how $\tilde{z}_{1,i+1,j}$ and $\tilde{z}_{2,i+1,j}$ can be computed. Equation (B1) can be discretized in the following way:

$$\frac{b\tilde{z}_{2,i+1,j}}{R_0} = \frac{b\tilde{z}_{2,i,j}}{R_0} - \frac{\Delta X}{2\Delta Y}\left(\frac{a\tilde{z}_{1,i,j+1}}{R_0} - \frac{b\tilde{z}_{1,i,j-1}}{R_0}\right) + \Delta X \, \mathcal{Z}_{0,i,j}$$

5   the error being proportionnal to ΔX. A boundary condition (for example $\tilde{z}_{2,i,-P} = 0$) is prescribed to end the computation. Knowing $\tilde{z}_{2,i+1,j}$, the value of $\tilde{z}_{1,i+1,j}$ is obtained by solving

$$\tilde{z}_{1,i+1,j}^2 + 2\tilde{z}_{1,i+1,j}(z_1^0 - w_1) + \tilde{z}_{2,i+1,j}^2 + 2\tilde{z}_{2,i+1,j}(z_2^0 - w_2) = 0 \tag{B3}$$

The computation of z_1^0 and z_2^0 would correspond to a solution such as $T_X = 0$ everywhere. The correction brought by $\tilde{z}_1$ and $\tilde{z}_2$ is associated with a mass transport perpendicular to the coast. As the latter in general is much smaller than the transport T_Y

10   parallel to the coast, it is expected that $\tilde{z}_1$ and $\tilde{z}_2$ are small in comparison with z_1^0 and z_2^0 (they are null at $X = 0$ and increase proportionally to the distance to the coast). In section 4.3, the approximate value of k associated with the solution z_1^0 is fully described.

Author contributions. MC provided the satellite analysis. JS made the numerical simulation. The manuscript benefitted from inputs of all the authors

15   *Competing interests.* The authors declare that they have no conflict of interest

Acknowledgements. We thank X. Capet for fruitful discussions, for his careful reading of the manuscript and pertinent comments. We thank R. Tailleux and J. Soares for their precise and constructive reviews which permitted to improve greatly this article.

References

Allen, J. S.: Some aspects of the forced wave response of stratified coastal regions. J. Phys. Oceanorgr., Vol 6, 113-119, 1976.

Batteen, M. L.: Wind-forced modeling studies of currents, meanders, and eddies in the California Current System, J. Geophys. Res., 102, 985–1009, 1997.

Capet, X., McWilliams, J., Molemaker, M., and Shchepetkin, A.: Mesoscale to submesoscale transition in the California current system: flow structure, eddy flux, and observational tests, J. Phys. Oceanogr., Vol 28, 29-43, 2008a.

Capet, X., McWilliams, J., Molemaker, M., and Shchepetkin, A.: Mesoscale to submesoscale transition in the California current system: Frontal processes. J. Phys. Oceanogr., Vol 28, 44-64, 2008b.

Capet, X., Estrade, P., Machu, É., Ndoye, S., Grelet, J., Lazar, A., Marié, L., Dausse, D., and Brehmer, P.: On the dynamics of the southern Senegal upwelling center; Observed variability from synoptic to superinertial scales, J. Phys. Oceanogr., Vol 47, 155-180, DOI: 10.1175/JPO-D-15-0247.1, 2017.

Castelao, R. M., and Bart, J. A.: Upwelling around Cabo Frio, Brazil: The importance of wind stress curl, Geophys. Res. Letters, Vol. 33, L03602, DOI: 10.1029/2005GL025182, 2006.

Clarke, A. J.: Wind forced linear and nonlinear Kelvin waves along an irregular coastline, J. Fluid Mech., Vol 83, 337-348, 1977.

Clarke, A. J.: The reflection of equatorial waves from ocean boundaries, J. Phys. Oceanorgr., Vol 13, 1193-1207, 1983.

Clarke, A. J., and Shi, C.: Critical frequencies at ocean boundaries. J. Geophys. Res., Vol 96, C6, 10731-10738, 1991.

Crépon, M., Richez, C.: Transient upwelling generated by two dimensional atmospheric forcing and variability in the coastline, J. Phys. Oceanogr., Vol 12, 1437-1457, 1982.

Crépon, M., Richez, C., and Chartier, M.: Effects of coastline geometry on upwellings, J. Phys. Oceanorgr., Vol 14, 1365-1382, 1984.

Demarcq, H., and Faure V.: Coastal upwelling and associated retention indices from satellite SST. Application to Octopus vulgaris recruitment, Oceanogr. Acta, 23, 391–407, 2000.

Diakhaté, M., de Coëtlogon, G., Lazar, A., Gaye, A.T., 2016: Intraseasonal SST variability within tropical Atlantic upwellings, *Q. J. R. Meteoror. Society*, 14, 372-386.

Enriquez, A. G., and Friehe, C. A.: Effects of wind stress and wind stress curl variability ob coastal upwelling. J. Phys. Oceanorgr., 25, 1551-1571, 1995.

Farikou, O., Sawadogo, S., Niang, A., Brajard, J., Mejia, C., Crépon, M., and Thiria, S.: Multivariate Analysis of the Senegalo-Mauritanian Area by Merging Satellite Remote Sensing Ocean Color and SST Observations, Research Journal of Environmental and Earth Sciences, 5(12), 756-768, 2013.

Farikou, O., Sawadogo, S., Niang, A., Diouf, D., Brajard, J., Mejia, C., Dandonneau, Y., Gasc, G., Crépon, M., and Thiria, S.: Inferring the seasonal evolution of phytoplankton groups in the Senegalo-Mauritanian upwelling region from satellite ocean-color spectral measurements. Journal of Geophysical Research. Oceans, 120 (9), pp. 6581-6601, DOI: 10.1002/2015JC010738, 2015.

Février S., J. Sirven, C. Herbaut, 2007: Interaction of a coastal Kelvin wave with the mean state in th Gulf Stream separation area. *J. Phys. Oceanorgr.*, 37, 1429-1444.

Gill, A. E., and Clarke, A. J.: Wind-induced upwelling, coastal currents and sea level changes. Deep Sea Res., 21, 325-345, 1974.

Grimshaw, R., and Allen, J. S.: Low frequency baroclinic waves off coastal boundaries, J. Phys. Oceanorgr., 18, 1124-1143, 1988.

Kounta, L., Capet, X., Jouanno, J., Kolodziejczyk, N., Sow, B., and Gaye, A. T.: A model perspective on the dynamics of the shadow zone of the eastern tropical Atlantic - Part 1: the poleward slope currents along West Africa, Ocean Sci., 14, 971-997, https://doi.org/10.5194/os-14-971-2018, 2018.

Lachkar, Z., and Gruber, N.: A comparative study of biological production in eastern boundary upwelling systems using an artificial neural network, Biogeosciences, 9, 293-308, doi: 10.5 194/bg-9-293-2012, 2012.

Lachkar, Z., and Gruber, N.: Response of biological production and air-sea CO_2 fluxes to upwelling intensifications in the California and Canary Current Systems, J. Mar. Syst., 109-110, 149-160, DOI : 10.1016/j.jmarsys.2012.04.003, 2013.

Lathuillière, C., Échevin, V., and Lévy, M.: Seasonal and intraseasonal surface chlorophyll-a variability along the northwest African coast. J. Geophys. Res., 113, C05007, doi: 10.1029/2007JC004433, 2008.

Marchesiello, P., McWilliams, J. C., and Shchepetkin, A.: Equilibrium structure and dynamics of the California current system, J. Phys. Oceanogr., 33, 753-783, 2003.

Marchesiello, P., and Estrade, P.: Eddy activity and mixing in upwelling systems: a comparative study of Northwest Africa and California regions, Int. J. Earth. Sci. (Geol Rundsch), 98, 299, https://doi.org/10.1007/s00531-007-0235-6, 2009.

McCalpin, J. D.: Rossby wave Generation by poleward propagating Kelvin waves: the midlatitude quasigeostrophic approximation, J. Phys. Oceanogr., 25, 1415-1425, 1995.

McCreary, J. P.: A linear stratified ocean model of the coastal undercurrent, Phil. Trans. Roy. Soc. Lond., A202, 385-413, 1981.

McCreary, J. P., and Kundu, P. K.: Western boundary circulation driven by an alongshore wind; With application to the Somali Current system, J. Mar. Res., 43, 493-516, 1985.

McCreary, J. P., Shetye, S. R., and Kundu, P. K.: Thermohaline forcing of eastern boundary currents: with application to the circulation off the west coast of Australia, J. Mar. Res., 44, 71-92, 1986.

Moore, D. W.: Planetary-gravity waves in an equatorial ocean, Ph. D. thesis, 201 pp., Harvard Univ., Cambridge, Mass., 1968.

Ndoye S., Capet, X., Estrade, P., Sow, B., Dagorne, D., Lazar, A., Gaye, A., and Brehmer, P.: SST patterns and dynamics of the Southern Senegal-Gambia upwelling center, J. Geophys. Res. Oceans, 119, 8315–8335, DOI:10.1002/2014JC010242, 2014.

Pickett, M. H., and Paduan, J. D.: Ekman transport and pumping in the California current based on the U.S. Navy's high-resolution atmospheric model (COAPMPS), J. Geophys. Res., 108, NO. C10, doi:10.1029/2003JC001902, 2003.

Richez, C., Philander, G., and Crépon, M.: Oceanic response to coastal winds with shear, Oceanologica Acta, 7, 4, 409-416, 1984.

Sadourny, R.: The dynamics of finite difference models of the shallow water equations, J. Atmos. Sci., 32, 680-689, 1975.

Sawadogo, S., Brajard, J., Niang, A., Lathuilieѐre, C., Crépon, M., and Thiria S.: Analysis of the Senegalo-Mauritanian upwelling by processing satellite remote sensing observations with topological maps, Proceedings IEEE International Joint Conference on Neural Networks, IJCNN, pp. 2826–2832, Atlanta, USA, 2009.

Schopf, P. S., Anderson, D. L. T., and Smith, R.: Beta-dispersion of low-frequency Rossby waves, Dyn. Atmos. Oceans, 5, 187-214, 1981.
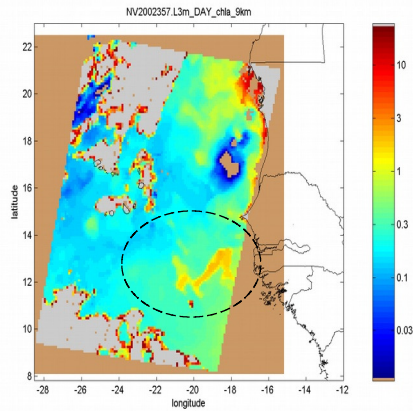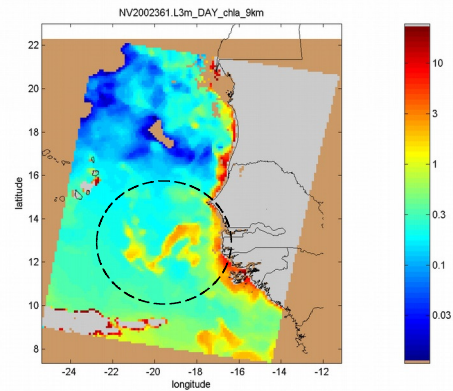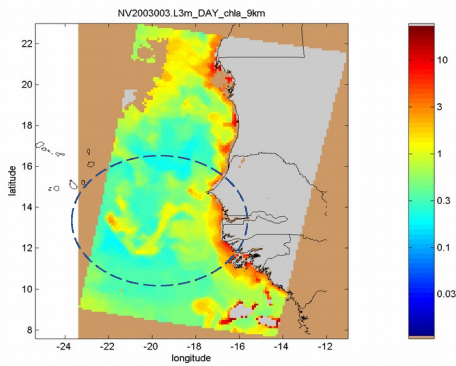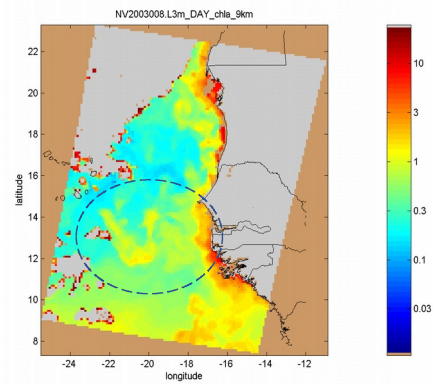
Figure 1. Chlorophyll observed by SEAWIFS at four different days. A wave-like pattern (which is circled by a dashed line) is visible between $-22°$ and $-18°$ in longitude and $-12°$ and $-14°$ in latitude. At the end of the period a westward propagation seems to initiate. The chlorophyll concentration is given in mg m^{-3} by the color bar at the right of the maps.
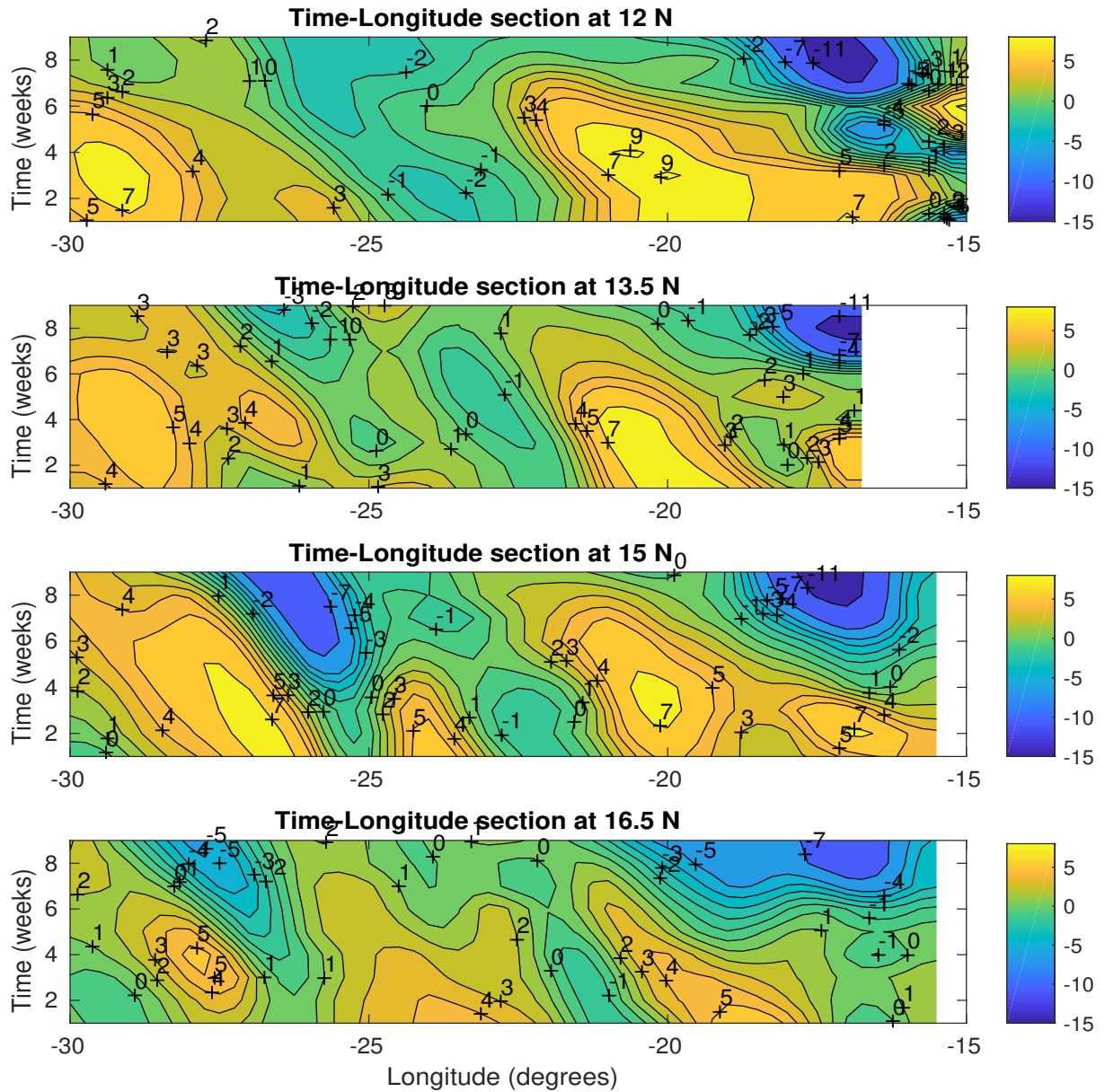
Figure 2. Hoevmuller diagrams of the SSH at latitudes 12°N, 13.5°N, 15°N, and 16.5°N (the SSH amplitude is given in cm by the color bar at the right of the diagrams). Note the decrease of the amplitude at 16.5°N. The phase velocity of the wave is about 4.5 cm/s.
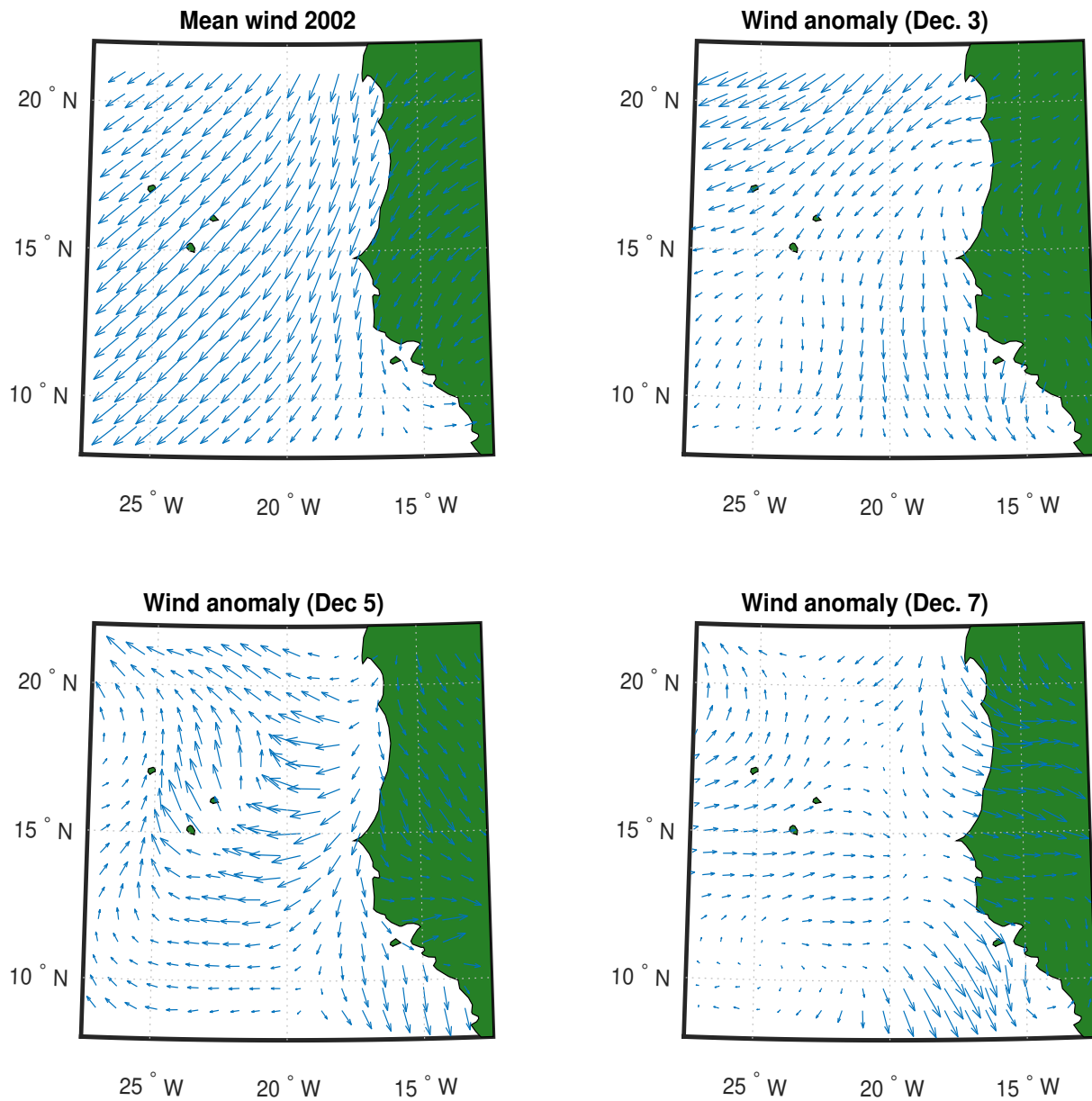
Figure 3. Mean wind velocity in December 2002 (maximum $\simeq 8$ m s^{-1}) and wind velocity anomaly in December 3, 5, and 7 (maximum $\simeq 4$ m s^{-1}).
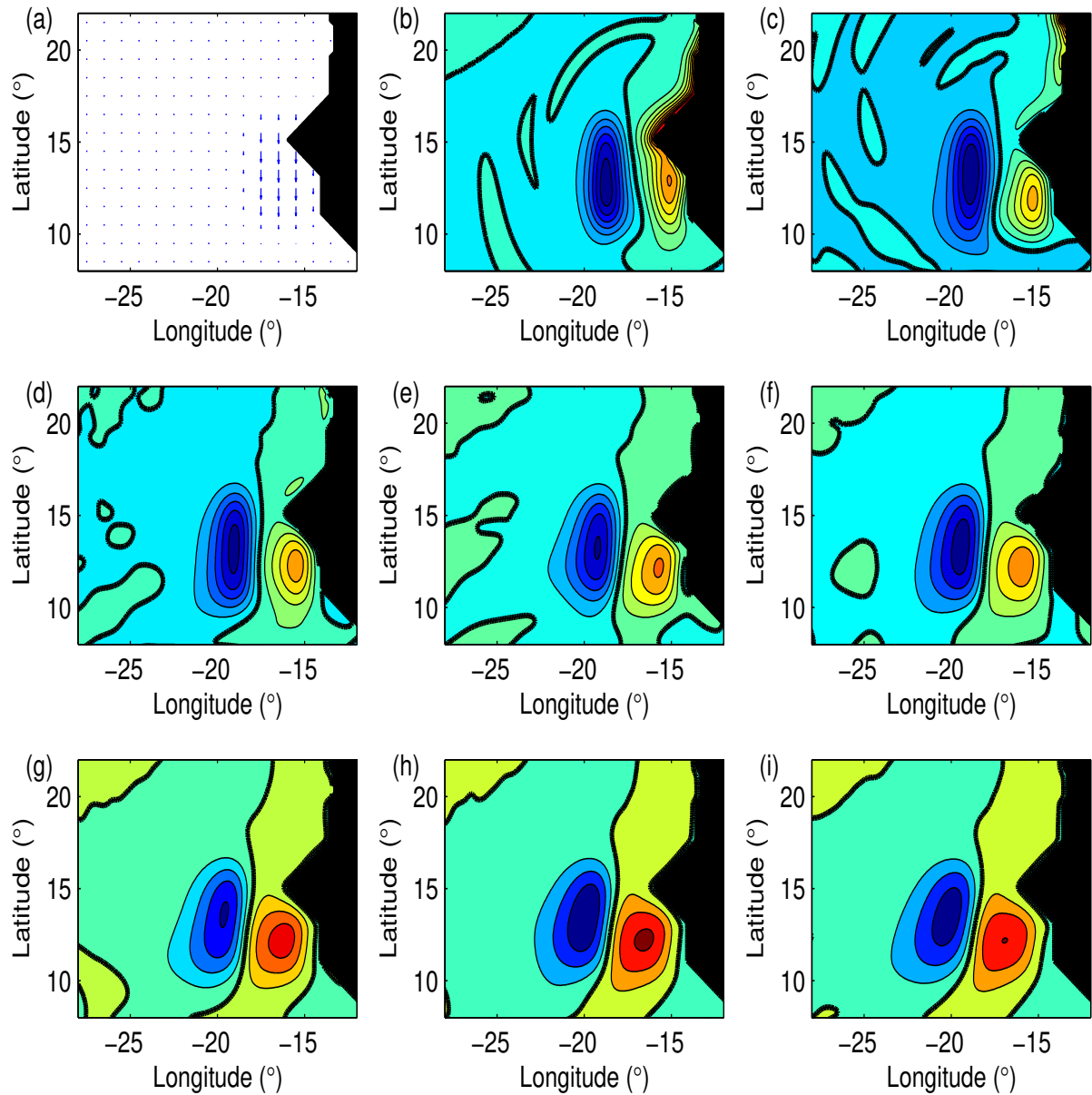
Figure 4. Response of the ocean to an anomalous wind stress applied during five days (panel (a)) and corresponding evolution of the active layer thickness for every five days from the close of the the wind stress anomaly up to 35 days after (panels from (b) to (i)). A Rossby wave is generated and a Kelvin wave quickly propagates along the coast. The Rossby wave propagates westward and its amplitude is divided by two between the first and the last panel. The 0 m isoline is indicated in bold; the isoline interval is 0.5 m (blue: negative).
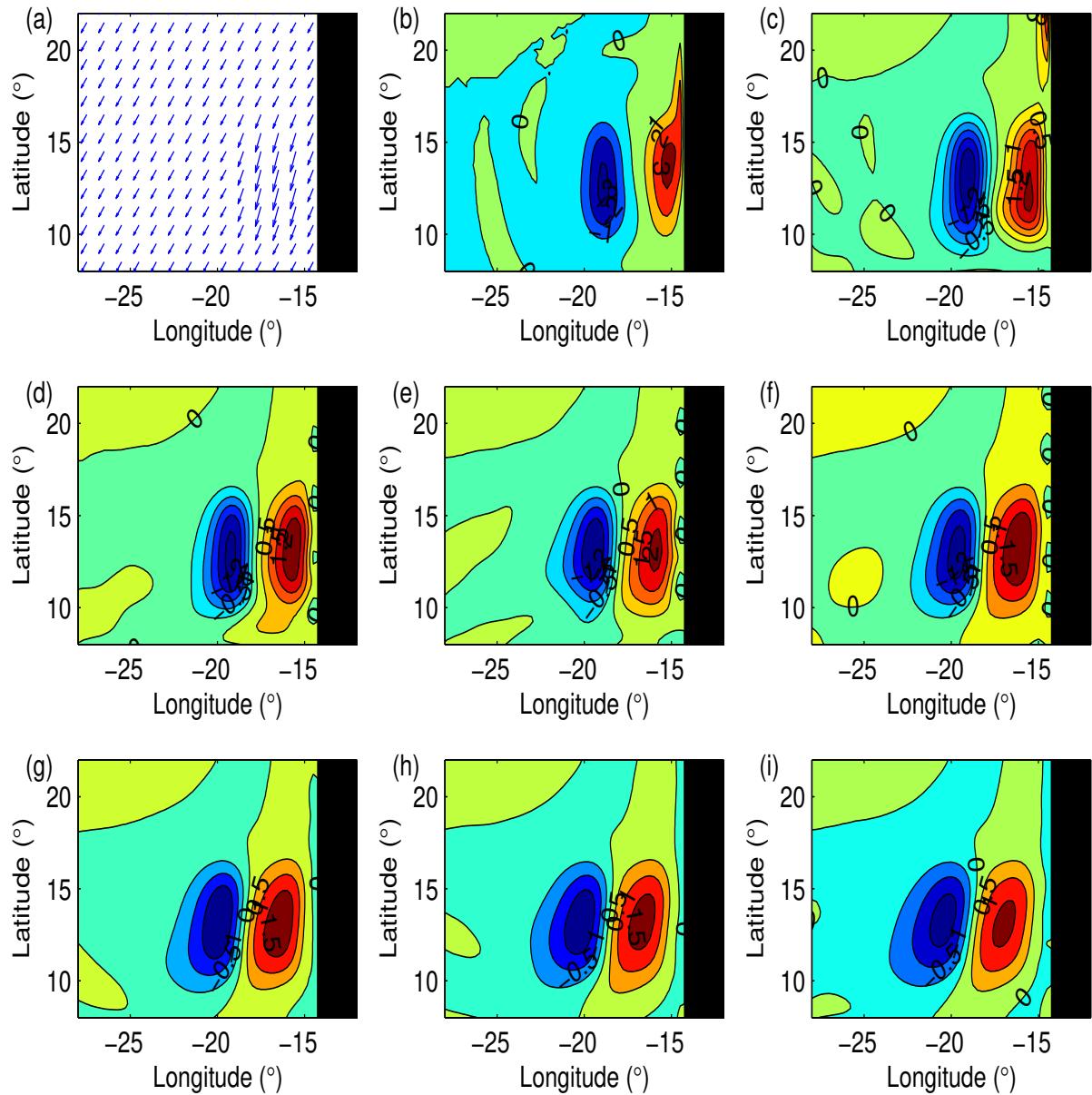
Figure 5. Solution obtained for the same conditions as in Fig. 4 for a straight coastline. Note that the mean wind stress is added to the wind stress anomaly in panel (a). A Rossby wave is still generated but the halting of the signal due to the cape is no longer observed. The latitudinal extent of the wave east of 19°W is thus nearly twice larger than in the previous case.
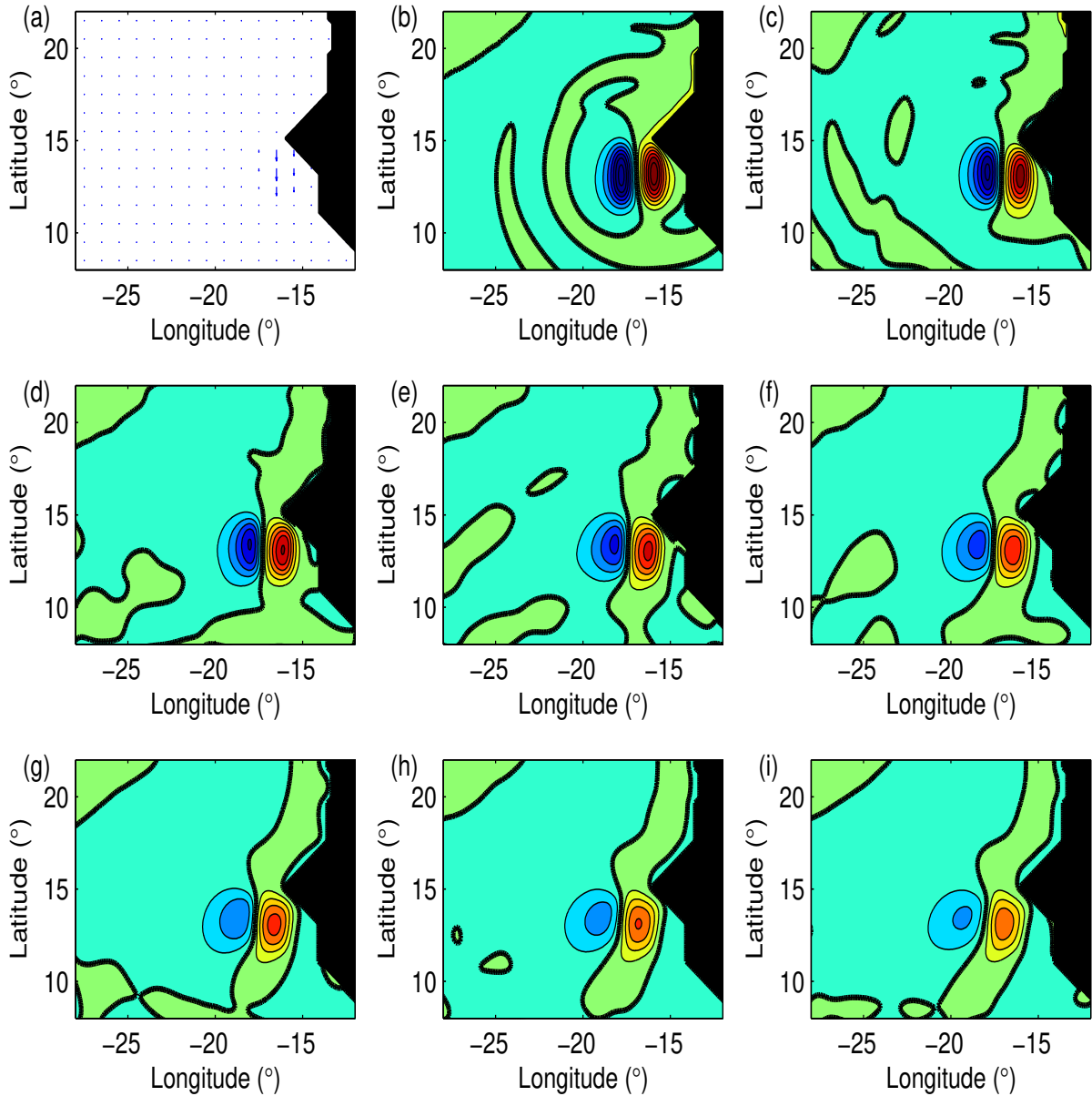
Figure 6. The wind anomaly extent is four times smaller than the one used in Figure 4 and the position of the center is kept unchanged (panel (a)). It still acts during five days and as previously the active layer thickness is shown for every five days from the close of the the wind stress anomaly up to 35 days after. A Rossby wave is generated and its extent is approximately four times smaller than previously. No Kelvin waves are created. The 0 m isoline is indicated in bold; the isoline interval is 0.5 m (blue: negative).
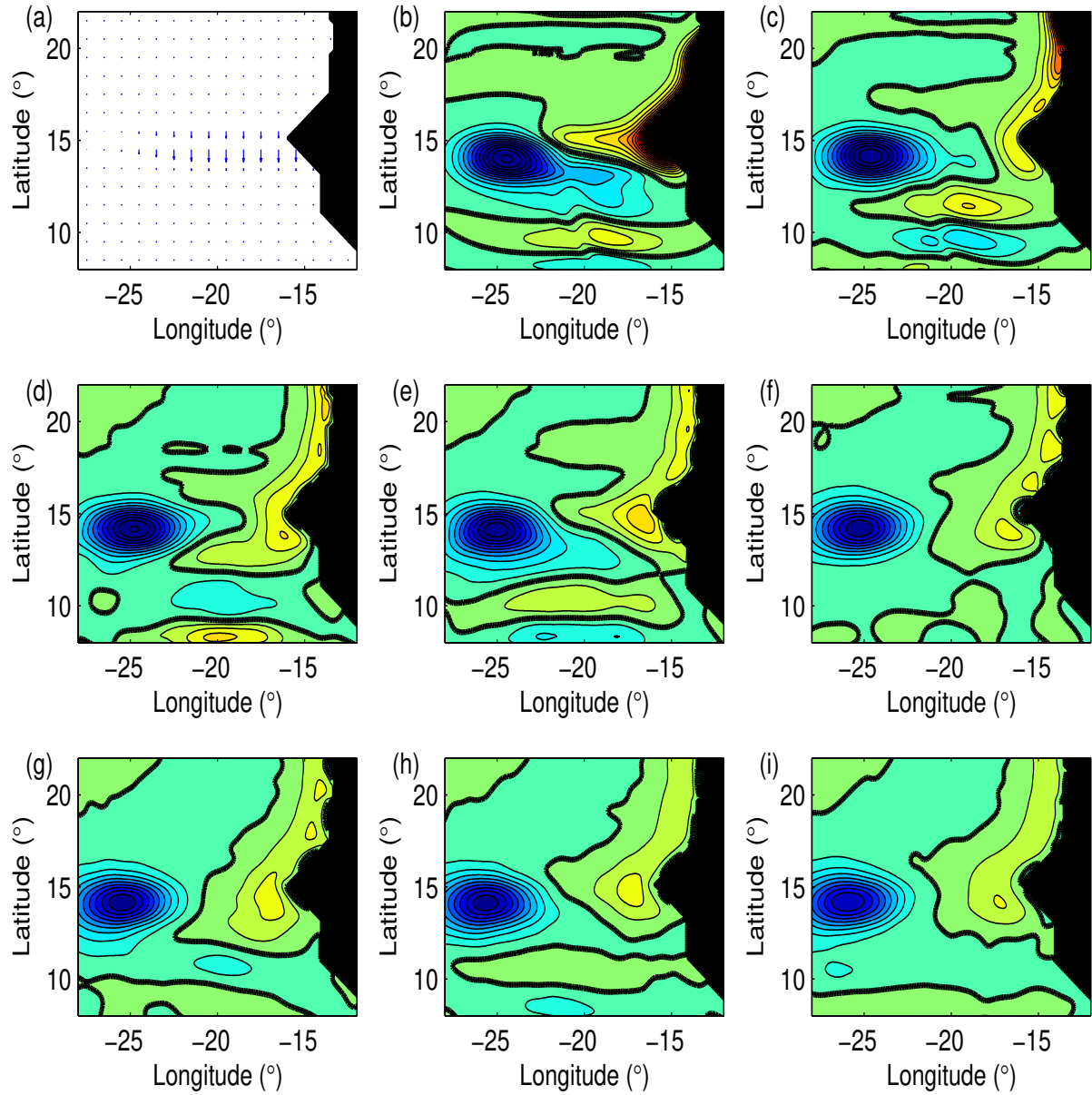
Figure 7. The wind anomaly now acts over a long (1000 km) and narrow (200 km) domain south of the cape during five days (panel (a)). The solution after the close of the wind burst is shown. A wave is generated but the anomaly remains moderate near the coast. The 0 m isoline is indicated in bold; the isoline interval is 0.1 m (blue: negative).
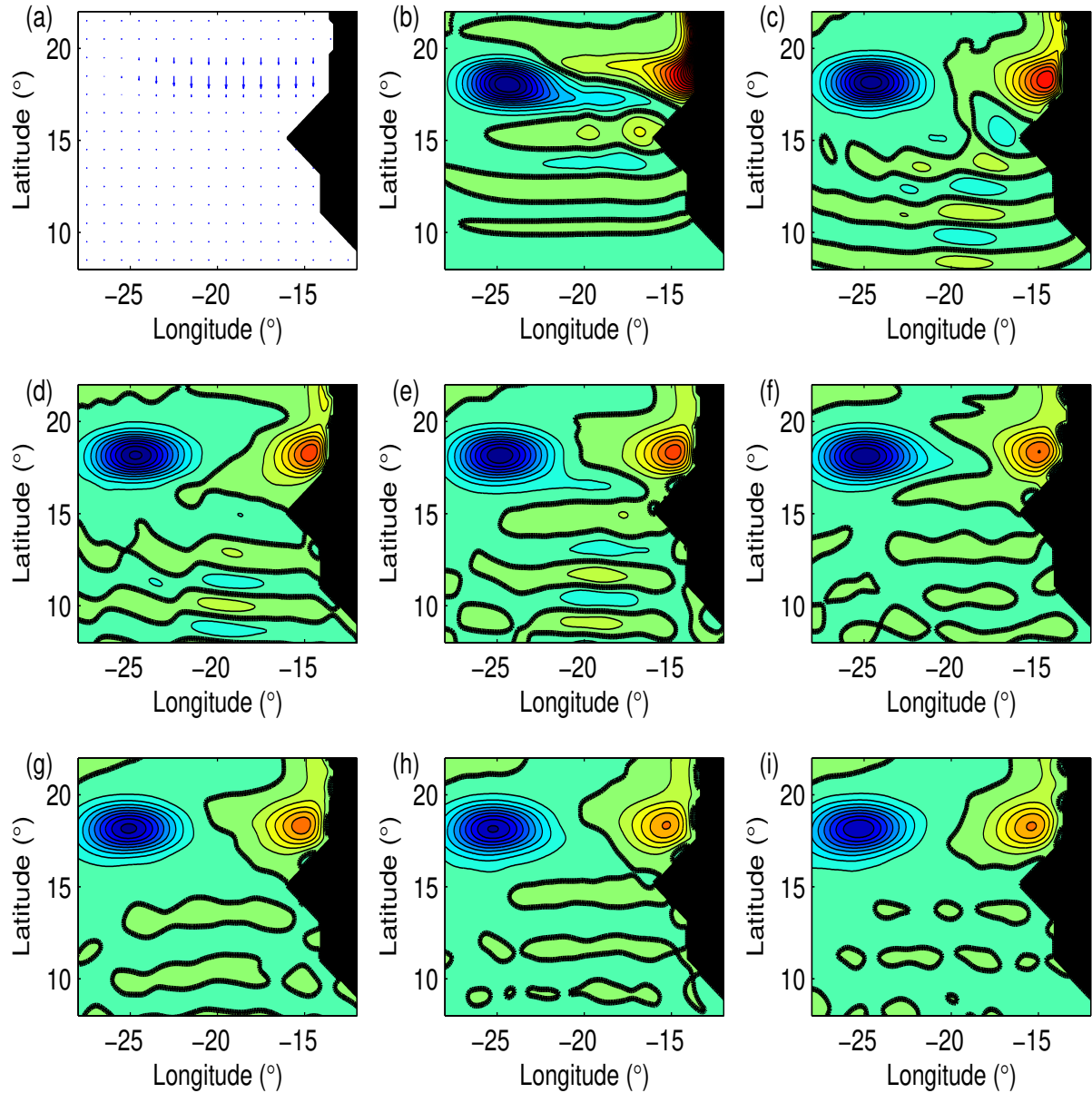
Figure 8. The wind anomaly now acts over a long (1000 km) and narrow (200 km) domain north of the cape during five days (first panel). The solution after the close of the wind burst is shown. A wave is generated and the anomaly near the coast has an amplitude comparable with the anomaly around 25° W. The 0 m isoline is indicated in bold; the isoline interval is 0.1 m (blue: negative).
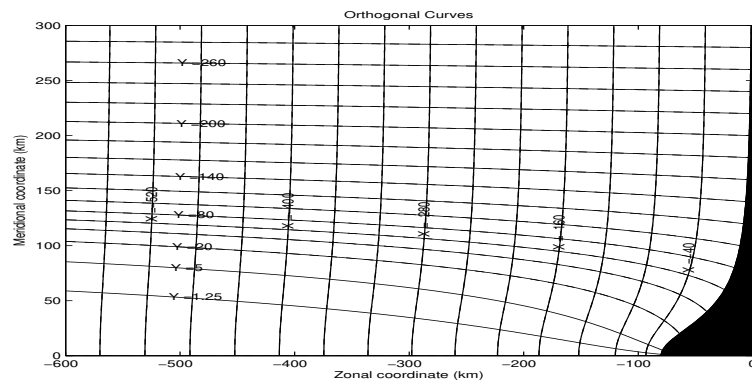
Figure 9. Example of orthogonal coordinates $\mathcal{X}$ and $\mathcal{Y}$ defined for a cape protruding from the coast into the sea over a distance of 80 km. Several values of $\mathcal{X}$ and $\mathcal{Y}$ have been indicated. Only one half of the domain has been represented.
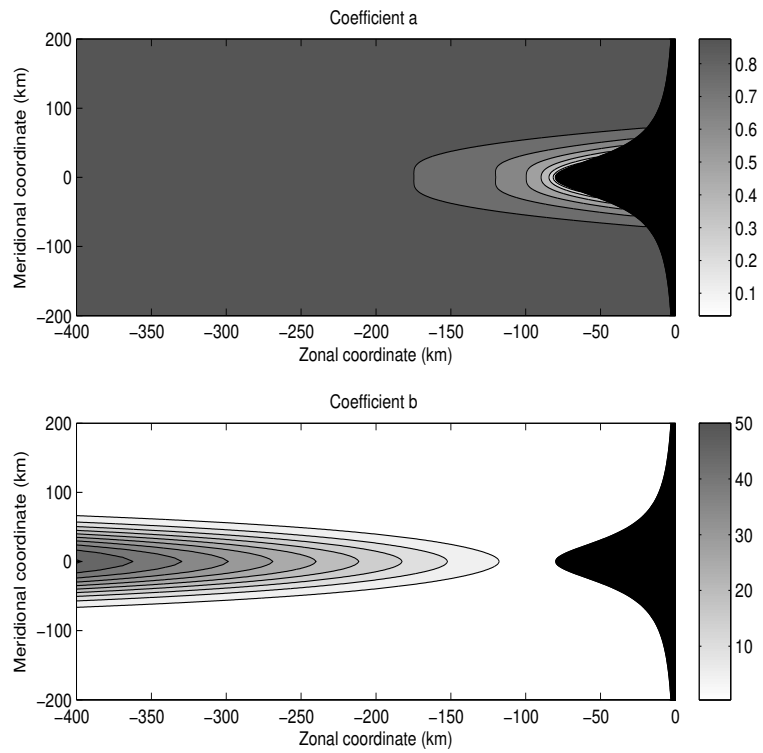
Figure 10. The coefficients a and b are given for the coordinate system of Figure 9 (they have no dimension).
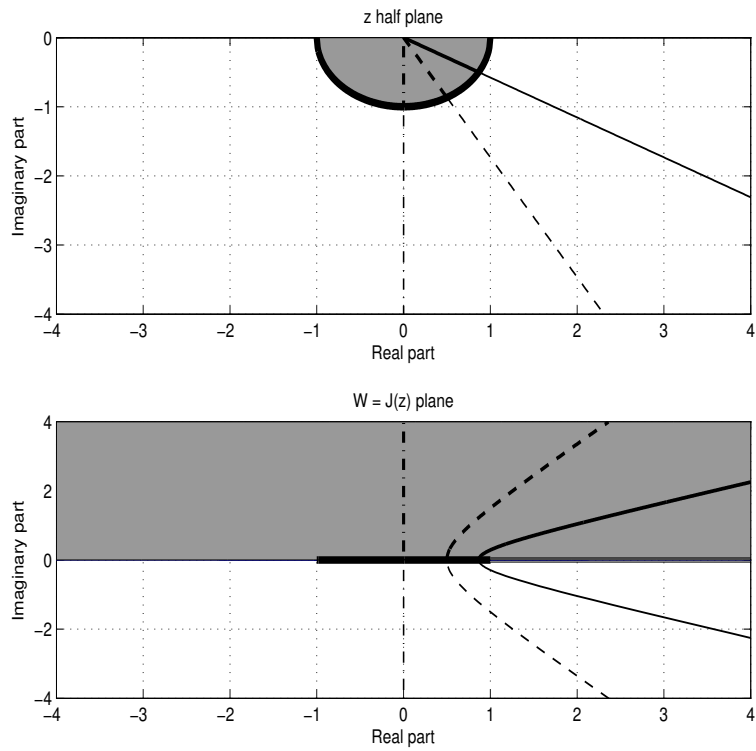
Figure 11. In top panel, the half complex plane $\Im(z) \leq 0$ with $z = \xi z_1$ is shown. The domain is restricted to complex numbers with a negative imaginary part since $k_I = a\Im(z)/(\xi R_0)$ must be negative. The half circle $|z| = 1$ and a few straight lines have been drawn. In botton panel the Joukowsky transform of the previous half plane $W = J(z)$ is shown. The segment $[-1, 1]$ is the image of the half circle. The upper (lower) half plane corresponds to the image of its interior (exterior). The image of the straight lines are correspondingly represented.
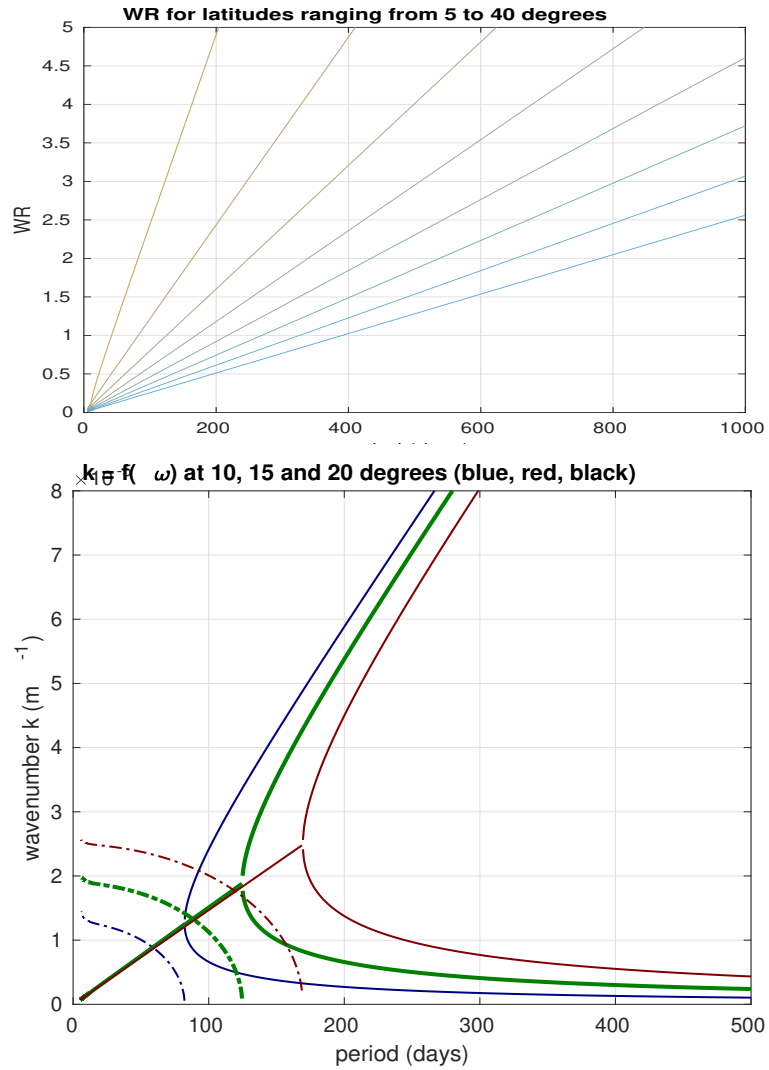
Figure 12. Top panel: W_R is shown for latitudes ranging from $5°$N (left segment) to $40°$ N (right segment). The critical value $W_R = 1$ is reached at $15°$ N for a period of about 125 days. Bottom panel: wavenumber k as a function of the period T for three different latitudes ($10°$ (blue), $15°$ (red), and $20°$).
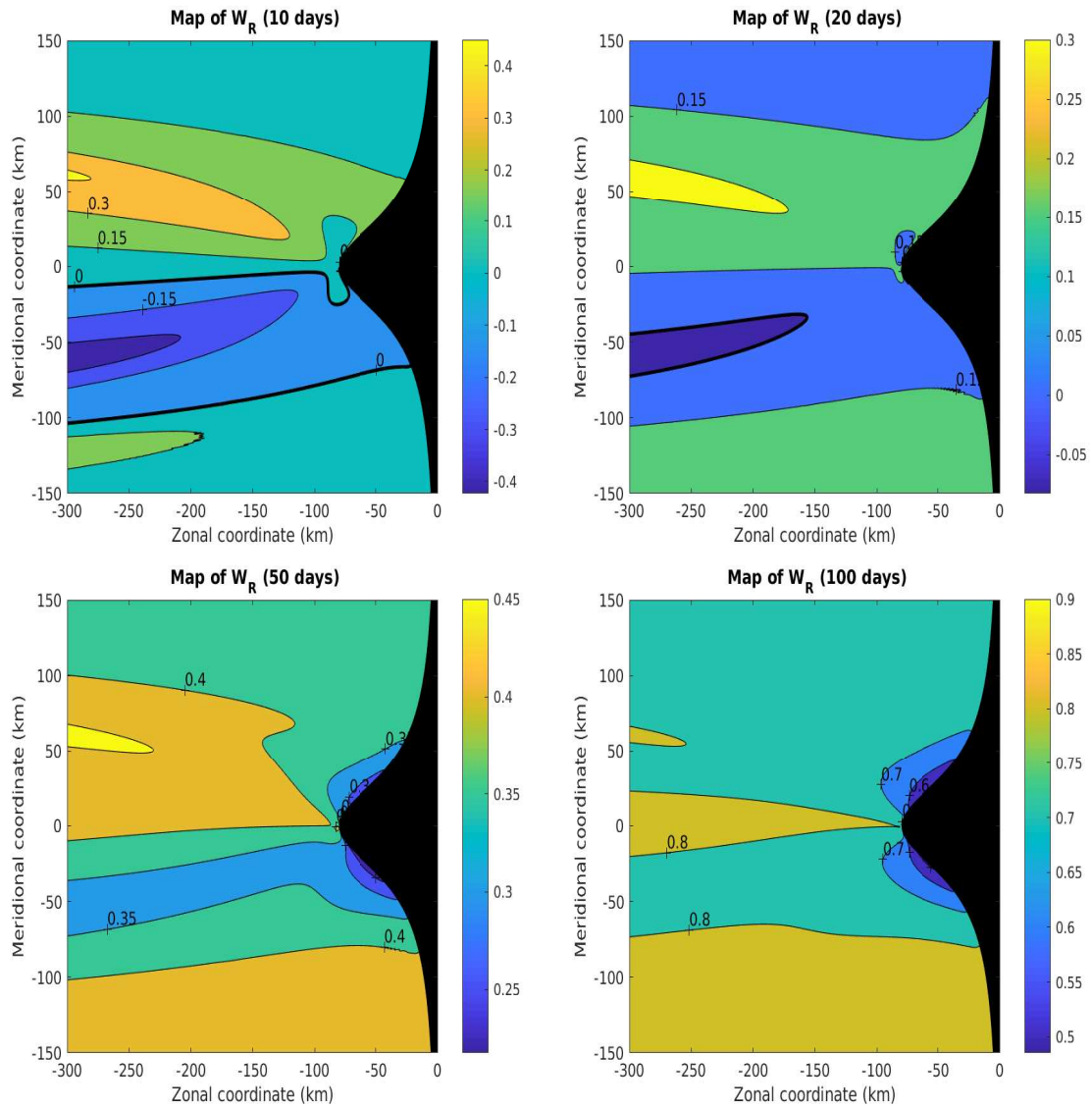
Figure 13. Dimensionless coefficient W_R for periods equal to 10 days, 20 days, 50 days, and 100 days. The bold black line corresponds to $W_R = 0$. When the period of the wave shortens (smaller than 20 days), W_R becomes negative in a narrow band south of the cape. For period longer than 100 days, the diagram is nearly symmetric.
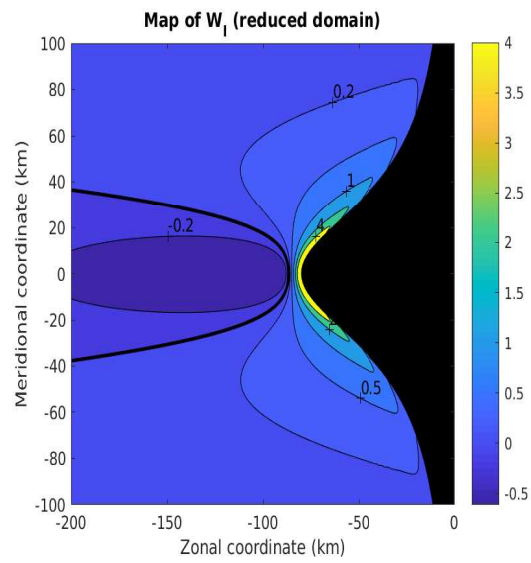
Figure 14. Dimensionless coefficient W_I. It is independent of the period of the wave. Note that the domain is reduced in comparison with the previous figure.
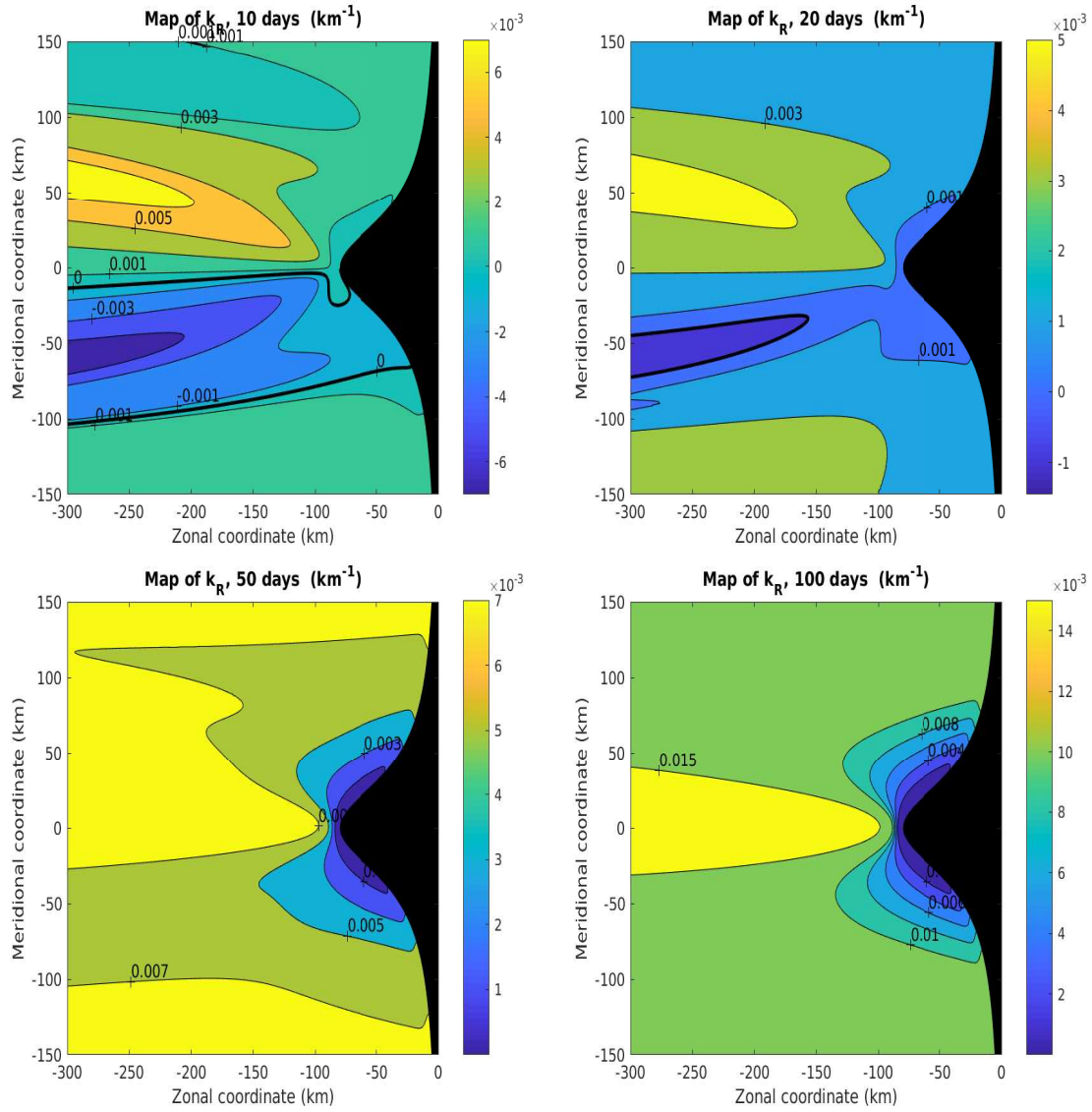
Figure 15. Coefficient k_R for periods equal to 10 days, 20 days, 50 days, and 100 days. The bold black line separates postive from negative values. Where W_R is negative, k_R is negative (for periods shorter than 20 days, in the area located to the south of the cape).
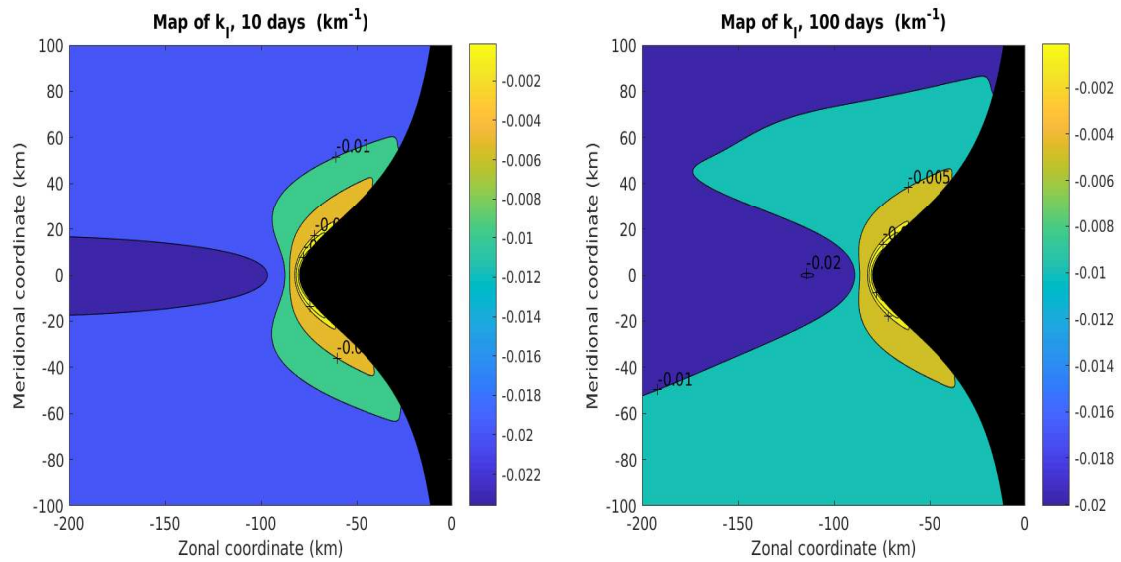
Figure 16. Coefficient k_I for periods equal to 10 days and 100 days. This coefficient weakly depends on the period of the wave.